Thin-Walled Structures

Local Buckling Strength and Design of Cold-Formed Steel Beams with Slotted Perforations

Natalia Degtyareva
Institute of Architecture and Construction, South Ural State University,
Chelyabinsk, Russia.
Perampalam Gatheeshgar
Faculty of Engineering and Environment, Northumbria University,
Newcastle, UK.
Keerthan Poologanathan
Faculty of Engineering and Environment, Northumbria University,
Newcastle, UK.
Shanmuganathan Gunalan
School of Engineering and Built Environment, Griffith University,
Gold Coast, QLD, 4222, Australia.
Islam Shyha
Faculty of Engineering and Environment, Northumbria University
Newcastle, UK.
Alex McIntosh
Faculty of Engineering and Environment, Northumbria University
Newcastle, UK.

Abstract

Providing staggered slotted perforations to the Cold-Formed Steel (CFS) beams is a new approach being used in light gauge steel construction aiming to enhance both the fire and energy performances. However, slots in the web reduce the load-bearing capacity of CFS beams and existing studies do not provide a definite evaluation of the design expressions to determine the structural performance of slotted perforated CFS flexural members. Therefore, the present study aims to establish a methodology to determine the flexural capacity of staggered slotted perforated CFS beams subject to local buckling through developing three-dimensional Finite Element (FE) models. The developed FE models were subjected to validation against the related test data. Subsequently, the validated FE model was employed to conduct further parametric studies (432 FE models). Parameters include the dimensions of the CFS beams and staggered slotted perforations, rows and row groups of slots and yield strength. The effect of these factors on the local buckling capacity of the staggered slotted perforated CFS beams under bending is discussed. The paper concludes with a proposal of Direct Strength Method (DSM) based new design equations to predict the bending capacity of the CFS beams

with staggered slotted perforations subject to local buckling and to enhance their commercial aspects.

Keywords: Cold-formed Steel; Staggered Slotted Perforations; Flexural Capacity; Local Buckling; Finite Element Analyses; Direct Strength Method; New Design Equations.

1 Introduction

Cold-Formed Steel (CFS) structural elements have been extremely widespread in building applications for many decades now. However, the advancements achieved in manufacturing technologies and demand for a more efficient system keep revising the CFS members in terms of shape and configurations. One such modification is introducing staggered slotted perforations to the CFS webs aiming to enhance the thermal effectiveness. Fig. 1 depicts the real world application of the slotted perforated CFS beams in construction, while Fig. 2 shows how the thermal transmittance becomes effective when compared to the solid web CFS sections. Many research studies have highlighted the advantages of slotted perforated webs, these include reduced thermal bridging effect, cost-effectiveness and, improved energy performance [1-4]. However, attention needs to be given to staggered slotted perforated CFS channels, as the reduction of the web area affects the load-carrying capacity.

Kesti [5] conducted an experimental and theoretical study to investigate the local and distortional buckling of CFS wall studs and based on the results, developed design guidelines for compressed web perforated steel wall studs. Similar to the wall studs, staggered slotted perforation can be provided to CFS beams for improving the thermal performance of the floor panels. In this case, the degree of effect on the structural performance needs to be examined carefully under particular loading scenarios such as bending, shear, web crippling actions and combined actions. The presence of the staggered slotted perforations resulted in up to 70% shear capacity reduction compared to the solid CFS beams [6, 7]. In addition, combined bending and shear behaviour of CFS beams with staggered slotted perforations has also been investigated by Degtyareva et al. [8] and new design proposals were also reported in that study. Despite extensive research studies have been conducted to investigate the flexural behaviour of the CFS beams subject to distortional and local buckling, to date, no research has focused on assessing the reduction in bending capacity due to the presence of the staggered slotted perforations.

Yu and Schafer [9, 10] and Pham and Hancock [11] performed distortional and local buckling test on cold-formed Z-and C-section beams and investigated the reliability of the Direct Strength Method (DSM) design. Additionally, Siahaan et al. [12-14] studied the local buckling strength and behaviour of the innovative rivet fastened rectangular hollow flange beams through an experimental and numerical approach. A reduction factor based design equation was proposed to determine the ultimate bending capacity subject to local buckling. In comparison to the aforementioned studies on solid web CFS beams, flexural behaviour of CFS beams with rectangular web openings subject to distortional [15, 16] and local buckling [16] have been investigated both experimentally and numerically. Modified DSM based design equations have been proposed to account the influence of unstiffened rectangular web opening on the bending capacity. Recent research studies have focused on deriving an analytical solution to determine the distortional buckling stress of CFS steel beams with web openings [17, 18]. Degtyareva [19] presented a review of the experimental study to determine the bending capacity of the CFS channels with the slotted webs. To date, no research has been reported on the bending strength and behaviour of staggered slotted perforated CFS beams subject to local buckling.

Therefore, the aim of this study described herein is to explore the ultimate bending capacity of the CFS beams with staggered slotted perforations subject to local buckling. Finite Element (FE) models were developed and validated against the relevant test results. Validated FE models were used in a parametric analysis varying the influencing parameters. Furthermore, the current DSM equations for local buckling were extended to cover CFS beams having staggered slotted perforations.

2 FE modelling of slotted perforated CFS channels

2.1 General

The general purpose and commercially available FE package ANSYS [20] has been employed to generate three dimensional FE models of slotted perforated beams, which allow for local buckling. The developed FE models were ensured to fail prominently in local buckling through providing appropriate boundary conditions while the possibility of distortional buckling failure was effectively restricted. The local buckling and four-point bending tests were used to validate the FE models and subsequently in parametric studies. The load was applied through attaching

the 5 mm thickness Web Side Plates (WSPs) to the models whilst the end supports were also provided through attaching WSPs.

2.2 Element type and mesh refinement

CFS beams have negligible cross-sectional thickness compared to the other two dimensions. Therefore, shell element theory can be employed. SHELL 181 element available in the ANSYS element library was assigned to all components of the FE models (see Fig. 3). This SHELL 181 element has eight degrees of freedom at their four nodes. In addition, ANSYS shell element library also contains an eight-node shell element, SHELL 281, which has similar degrees of freedom in contrast to the number of nodes. However, both predicted the bending capacity subject to local bucking with similar accuracy, accounting geometrical and material non-linearity. Therefore, considering the computation time and available computing resources, SHELL 181 element was used for the analysis. In addition, the contact between WSP and CFS channel was modelled with CONTA173 and TARGE170 elements.

In a similar way, mesh size also affects the accuracy and time efficiency of FE models. All the components of the FE models were fully refined with 5 mm × 5 mm mesh sizes except the perforated web regions. Since the slotted perforated web region has been identified as critical, finer mesh refinement of 1.5 mm (in vertical direction) × 5 mm (in longitudinal direction) was given. Similar mesh sizes were also adopted to model the shear and combined bending and shear behaviour of CFS beams with slotted perforations [6, 8]. Furthermore, the selected mesh sizes produced a satisfactory agreement with test results, therefore, further refining procedure was not conducted.

2.3 Initial geometric imperfections

The technique of super positioning the scaled local buckling modes was followed to include the initial geometric imperfection shape and amplitude into FE simulation. Elastic buckling analysis was performed in ANSYS for the slotted perforated CFS channels to generate the local buckling mode in the pure bending region of the four-point bending model. Schafer and Peköz [21] represented the magnitude of the imperfections as a function of plate thickness, t. Therefore, a positive imperfection magnitude of 0.15t was used in the analysis and the lowest local buckling mode was used to introduce the shape of the initial geometric imperfection. The magnitude and shape were then fed into the non-linear analysis.

2.4 Material modelling

The material modelling defines the stress-strain behaviour of CFS with key parameters; yield strength, ultimate strength and modulus of elasticity. ANSYS provides several options to define the stress-strain relationship such as bi-linear and multi linear. Haidarali and Nethecot [22] investigated four different material models to identify the suitable stress-strain relationship for FE modelling. They concluded that strain hardening has negligible effect on the behaviour of CFS beams in FE modelling while the gradual yielding of the material is essential. However, in this study, thin-walled CFS beams were modelled as bi-linear isotropic hardening with von Mises yielding criteria. Thus only the yield stress and elastic modulus were inputted in FE modelling to define the stress-strain behaviour. Further, WSPs were modelled as an elastic material with continuously increasing stress. The bi-linear stress-strain behaviour for FE modelling of CFS beams showed good agreement in predicting the ultimate bending capacity within the validation process. Similar material modelling were also followed in parametric study. The residual stresses and the elevated yield strength at corner regions were ignored in the FE analysis as Schafer et al.[23] claimed that in general practice both effects counteract each other.

2.5 Boundary conditions

FE models were developed to provide simply supported boundary conditions to the four-point bending set-up. The simulated boundary conditions in the FE models for the validation phase is narrated in Fig. 4. The four-point bending test is a symmetric arrangement and hence, only half of the set-up was modelled with symmetric boundary conditions. The contact between the WSPs and the CFS beam was achieved considering the WSP and CFS beam as target and contact surfaces, respectively. The contact between WSP and CFS beam is standard contact with default settings. This also includes the effect of shell thickness. The friction factor was not inputted in between the WSP and CFS beam. Because, contact boundary conditions are adequate to restrict displacements of the CFS beam to the WSP direction. All the nodes in the WSP were restrained in x-direction. However, no restriction in z direction was provided. This is because ANSYS transforms symmetry boundary conditions to the restriction of displacements in the z direction and rotations about X and Y directions.The bolts, used to connect the WSP and CFS beam in tests, were simulated through coupling the WSP and CFS beam nodes at bolt locations. Here, translations of these nodes were coupled in the x, y, and z-directions. Location of the straps in the top and bottom flanges were simulated as boundary

conditions by restraining the translations and rotations of the strap locations at the top and bottom flanges nodes in the x and about z-directions, respectively. To prevent vertical movement of the end supports, the bottom edge mid-point in the WSP was restrained in the y-direction. Since WSP were attached to CFS beam, CFS beam has the capability to act as simply supported boundary conditions when suitable boundary conditions are provided to WSPs. Similar approach was followed in simply supported four-point bending tests of CFS beam [11]. Further, at the loading points, the rotations of the top edge of WSP nodes were coupled about the x-direction to ensure rotations of all nodes at the top edge of WPS are the same. This is because to avoid local deformations of the WSP at the loading point. The rotations of other directions were not coupled because the nodes will not rotate about y and z after restraining translations of all WSP nodes in x directions. Load was applied to the coupled node, where all the vertical displacements are coupled, as a displacement control approach. Displacement control approach was selected over load control approach as particularly in non-linear problems displacement-controlled method has a more extensive scope and powerful abilities.

2.6 Solution scheme

The linear perturbation analysis (linear buckling analysis) of the model was performed as the first step to obtain the local buckling shapes and eigenvalues of the 'perfect' CFS beams. The generated local buckling modes were then associated with the initial geometric imperfections. Following that, non-linear static analysis was performed with the input of the imperfection shape and magnitude from the linear perturbation analysis. For this non-linear static analysis, arc-length method was not considered. Because there will not be any convergence issues as contact elements are only used to restrict the displacement of CFS beam to WSP direction. The use of arc-length method is essential to overcome convergence issues when contact elements are used to apply loads. The sparse direct equation based non-linear static analysis in ANSYS considers the material yielding and large deformation effect under loading. It is noteworthy to mention that the loading was performed through displacement control approach.

2.7 Verification of the FE models

The developed FE models were verified against the available test results to ensure the selected element type, mesh, material model, boundary conditions and solution scheme are suitable for further study. For the verification, four-point bending test results reported by Pham and Hancock [11] was used. In that study, a total of 24 bending test were conducted to study the

behaviour of local and distortional buckling failure of cold-formed lipped channel and SupaCee sections. Local and distortional buckling tests have been classified by providing straps at regular intervals to the flanges in the pure bending region (mid-span) and providing no straps to the pure bending region, respectively. As this study focuses the local buckling behaviour of slotted perforated CFS beams under bending, six of these local buckling test results under bending for the lipped channel beams were verified with the FE analysis results. The imperfection magnitude of 0.15t with positive and negative values were used in FE analysis to determine the ultimate bending capacity.

Table 1 presents the comparison of the predicted bending capacity results from the FE analysis and test results. The comparison of the test results and FE analysis bending capacities showed a satisfactory agreement, with a mean value of 1.13 for both positive and negative imperfection magnitudes. In addition, the coefficient of variation (COV) values are 0.030 and 0.035 for positive and negative imperfection magnitudes, respectively. Table 1 also presents the FE results reported in Pham and Hancock's [24] numerical investigation for similar cross-section dimensions. Developed FE models using ANSYS showed a good agreement with the FE results reported in Pham and Hancock's [24] numerical study. It should be noted that the initial imperfection magnitudes for each CFS specimens were not measured in Pham and Hancock's [11] experiments. Therefore, the imperfection magnitude of 0.15t was used in the validation. FE analysis with zero imperfections ('perfect' CFS beams) resulted a mean value of 1.05 and COV value of 0.042. Thus, the tested CFS beams were more likely to be perfect sections. However, as a conservative approach, the imperfection magnitude of 0.15t was used in further parametric study. Fig. 5 shows the failure mode comparison between the local buckling test and FE models for C20015-Ms specimen. It can be noticed that the FE model predicted a similar failure mode in comparison to the test. For this specimen, the load-vertical displacement behaviour obtained from test and FE analysis is displayed in Fig. 6. Load-vertical displacement behaviour of the FE model also shows a consistent result at each stage compared to test curve. Therefore, the comparisons of the ultimate bending capacity, failure modes, and load-vertical displacement behaviour confirm that the selected model characteristics can be used to extend the FE analysis for slotted perforations.

Table 1: Comparison of FE results and experimental [11] bending capacities of solid CFS channels

Specimens	t (mm)	D (mm)	B_f (mm)	B_l (mm)	f_y (MPa)	Test (kNm)	$FE_{(0.15t)}$ (kNm)	$FE_{(-0.15t)}$ (kNm)	Test/ $FE_{(0.15t)}$	Test/ $FE_{(-0.15t)}$	$FE^*_{(0.15t)}$ (kNm)	$FE^*_{(-0.15t)}$ (kNm)	$FE^*_{(0.15t)}$ / $FE_{(0.15t)}$	$FE^*_{(-0.15t)}$ / $FE_{(-0.15t)}$
C15015-Ms	1.5	153.46	64.53	15.02	541.13	10.43	9.16	9.13	1.14	1.14	10.06	10.03	1.10	1.10
C15019-Ms	1.9	153.54	65.01	16.27	534.48	15.86	13.56	13.49	1.17	1.18	14.72	14.71	1.09	1.09
C15024-Ms	2.4	153.43	63.58	20.88	485.29	19.84	17.40	17.31	1.14	1.15	18.84	18.84	1.08	1.09
C20015-Ms	1.5	203.74	75.88	16.16	513.40	13.47	12.49	12.61	1.08	1.07	13.37	13.39	1.07	1.06
C20019-Ms	1.9	203.54	79.27	17.51	510.48	21.76	19.78	19.82	1.10	1.10	20.03	20.03	1.01	1.01
C20024-Ms	2.4	202.30	77.58	21.26	483.49	31.39	27.34	27.19	1.15	1.15	28.23	28.20	1.03	1.04
Min									1.08	1.07			1.01	1.01
Max									1.17	1.18			1.10	1.10
Mean									1.13	1.13			1.06	1.06
COV									0.030	0.035			0.032	0.033

Note: t = thickness; D= web depth, B_f= flange width, B_l= lip length; f_y= yield stress, FE* = FE values reported in [24] for similar dimensions

3 Extended finite element analysis

3.1 Aim of the extended analysis

Given the satisfactory verification of the developed four-point bending FE model, an extension to a greater variety of staggered slotted perforated CFS channels and yield mechanical properties is possible. Particular interest was given to examine all the influencing parameters on the local buckling strength and behaviour. This was mainly driven to create a wide range of data sets and from that develop simplified design equations to predict the ultimate bending capacity of the staggered slotted perforated CFS beams subject to local buckling. The modulus of the elasticity of the material is considered as 200 GPa and the Poisson's ratio was taken as 0.3, for both CFS channels and WSP.

3.2 Parameters of interest

All the dimensional parameters and the mechanical properties were varied, thus 432 discrete FE models of CFS beams with staggered slotted perforations were developed to generate the ultimate bending capacity data set. The dimensional parameters of section depth (D), flange width (B_f), lip length (B_l), thickness (t), slot length (L_{sl}), slot width (W_{sl}), total number of slot rows (n), number of slot row groups (N) were varied. Fig. 7 shows the definition of the notations used in the parametric study. Three different section depths of 150, 200, and 250 mm, two different flange widths of 45 and 65 mm, three different thicknesses of 1, 2, and 3 mm, two different slot lengths of 60 and 75 mm, two different slot widths of 3 and 5 mm, three different total number slot rows of 6, 8, and 12 (6 rows for 150 mm section depth, 6 and 8 rows for 200 mm section depth, and 6, 8, and 12 rows for 250 mm section depth), and two-slot row

groups were the considered dimensional parameters. To vary the mechanical properties, different yield strengths (f_y) were considered. Three different yield strengths of 300, 500, and 600 MPa were considered to cover the wide range of yield strength. The varying parameters are presented in Table 2. The developed 432 FE models were labelled with notations for better understanding. The labelling rule used in the parametric study is narrated in Fig. 8.

Table 2: Parametric study details

f_y (MPa)	D (mm)	B_f (mm)	B_l (mm)	t (mm)	L_{sl} (mm)	W_{sl} (mm)	n	N	Number of models
300	150	45	13	1, 2, 3	60, 75	3, 5	6	1, 2	24
	200	45	13	1, 2, 3	60, 75	3, 5	6, 8	1, 2	48
	250	65	13	1, 2, 3	60, 75	3, 5	6, 8, 12	1, 2	72
Sub-total									144
500	150	45	13	1, 2, 3	60, 75	3, 5	6	1, 2	24
	200	45	13	1, 2, 3	60, 75	3, 5	6, 8	1, 2	48
	250	65	13	1, 2, 3	60, 75	3, 5	6, 8, 12	1, 2	72
Sub-total									144
600	150	45	13	1, 2, 3	60, 75	3, 5	6	1, 2	24
	200	45	13	1, 2, 3	60, 75	3, 5	6, 8	1, 2	48
	250	65	13	1, 2, 3	60, 75	3, 5	6, 8, 12	1, 2	72
Sub-total									144
Total									432

Note: f_y = yield stress, D = section depth, B_f = flange width, B_l = lip length, t = thickness, L_{sl} = slot length, W_{sl} = slot width, n = total number of slot rows, N = number of slot row groups

3.3 Effect of FE model span

The validated FE models have a total span of 2600 mm as similar to the test spans used in [11]. However, this study has also focused on investigating the effect of the FE model span on the ultimate bending capacity. A few analyses were performed to investigate this considering two different spans, 2600 mm and 4800 mm. In addition to examining the effect of the total span, another important point considered is to provide the slotted perforations throughout the entire length or only to the pure bending span. To investigate this, the analysis was conducted in two categories. In the first category, the CFS beam was modelled as having a 4800 mm span and staggered slotted perforations incorporated along the entire web of the span. In contrast, in the second category, the CFS beam was modelled as having a 2600 mm span and staggered slotted perforations were incorporated only in web of the pure bending region (mid-span). Similarly, this approach of two varying spans were also checked for solid web CFS channels. Fig. 9

depicts the developed FE models of 4800 mm long solid web CFS beams and CFS beams with staggered slotted perforations provided along the entire span. In the developed FE models of 2600 mm span, solid web CFS beams and CFS beams with staggered slotted perforations were limited only to the mid-span are shown in Fig. 10. The boundary conditions used for these two categories are depicted in Figs. 11 and 12, respectively. The ultimate bending capacity obtained from the FE analysis for the different spans are presented in Table 3. The analysis results display that the perforations in the two end spans of four-point bending set-up and total span do not influence the ultimate bending capacity. Therefore, considering the time efficiency for the analysis, a span of 2600 mm with staggered slotted perforations only in the mid-span was used in the parametric study. Figs. 13 and 14 show the failure mode comparison obtained at different stages for 2600 mm and 4800 mm spans of 250-3-60-3-2-12-300, and 150-3-60-3-1-6-600 beams, respectively.

Table 3: FE ultimate bending capacity comparison for solid and slotted web CFS channels having different spans.

FE model (solid web)	$M_{solid,\ 4.8}$ (kNm)	$M_{solid,\ 2.6}$ (kNm)	$M_{solid,\ 4.8}$ / $M_{solid,\ 2.6}$	FE model (slotted web)	$M_{slots,\ 4.8}$ (kNm)	$M_{slots,\ 2.6}$ (kNm)	$M_{slots,\ 4.8}$ / $M_{slots,\ 2.6}$
150-1-0-0-0-0-600	4.83	4.79	1.01	150-1-60-3-1-6-600	4.75	4.75	1.01
150-3-0-0-0-0-600	19.92	19.66	1.01	150-1-60-3-2-6-600	4.67	4.67	1.01
250-1-0-0-0-0-600	8.10	8.09	1.00	150-3-60-3-1-6-600	18.76	18.76	0.98
250-3-0-0-0-0-600	45.15	45.46	0.99	150-3-60-3-2-6-600	18.56	18.56	0.98
150-1-0-0-0-0-300	3.19	3.17	1.01	250-1-60-3-1-6-600	8.05	8.05	1.00
150-3-0-0-0-0-300	10.49	10.40	1.01	250-1-60-3-2-6-600	8.10	8.10	1.03
250-1-0-0-0-0-300	5.55	5.55	1.00	250-1-60-3-1-12-600	7.82	7.82	0.99
250-3-0-0-0-0-300	25.52	25.69	0.99	250-1-60-3-2-12-600	7.76	7.76	0.99
				250-3-60-3-1-6-600	45.18	45.18	1.02
				250-3-60-3-2-6-600	44.53	44.53	1.01
				250-3-60-3-1-12-600	43.47	43.47	1.01
				250-3-60-3-2-12-600	42.51	42.51	1.01
				150-1-60-3-1-6-300	3.13	3.11	1.01
				150-1-60-3-2-6-300	3.10	3.09	1.00
				150-3-60-3-1-6-300	10.10	10.13	1.00
				150-3-60-3-2-6-300	9.99	10.05	0.99
				250-1-60-3-1-6-300	5.57	5.54	1.01
				250-1-60-3-2-6-300	5.52	5.52	1.00
				250-1-60-3-1-12-300	5.49	5.48	1.00
				250-1-60-3-2-12-300	5.50	5.47	1.01
				250-3-60-3-1-6-300	25.66	25.32	1.01
				250-3-60-3-2-6-300	25.42	25.24	1.01
				250-3-60-3-1-12-300	24.89	24.72	1.01
				250-3-60-3-2-12-300	24.44	24.32	1.00

Note: $M_{solid,\ 4.8}$ = bending capacity for 4800 mm span with solid web, $M_{solid,\ 2.6}$ = bending capacity for 2600 mm span with solid web, $M_{slots,\ 4.8}$ = bending capacity for 4800 mm span with slotted web, $M_{slots,\ 2.6}$ = bending capacity for 2600 mm span with slotted web

4 FE results analysis of the slotted perforated channels

The ultimate bending strength and behaviour of CFS beams with staggered slotted perforations were investigated in detail using the analysed 432 FE models. Further, the ultimate bending capacity of the corresponding solid web CFS channels were also obtained from FE analysis to study the bending capacity reduction due to the staggered slotted perforations. These results are required to develop simplified design equations, explained in the following sections. Therefore, the bending capacities, section and elastic properties of the solid web CFS channels were determined and presented in Table 4. Here, the local buckling moment was calculated from THIN-WALL finite strip analysis software.

Table 4: Section and elastic properties of the solid web CFS channels

D (mm)	B_f (mm)	B_l (mm)	t (mm)	Z (mm^3)	S (mm^3)	S/Z	M_{ol} (kNm)
150	45	13	1	11 416	13 812	1.21	2.90
			2	21 416	26 945	1.26	22.37
			3	30 024	39 404	1.31	66.02
200	45	13	1	17 018	20 987	1.23	2.54
			2	32 199	41 094	1.28	19.36
			3	45 567	60 329	1.32	60.98
250	65	13	1	28 416	34 393	1.21	2.64
			2	54 495	67 644	1.24	20.29
			3	78 260	99 824	1.28	62.50
Mean						1.26	

Note: D = section depth, B_f = flange width, B_l = lip length, Z = elastic section modulus, S = plastic section modulus, M_{ol} = local buckling moment

Fig. 15 details the load- vertical displacement response of slotted channel 150-2-75-3-2-6-300, its corresponding solid channel 150-2-0-0-0-0-300 and its behavior at different stages. Similarly, the load-deflection response of slotted channel 200-2-75-3-2-8-500, and its corresponding solid channel 200-2-0-0-0-0-500 and its behavior at different stages are illustrated in Fig. 16. Fig. 17 shows the von Misses stress failure pattern for a 150 mm section depth solid and staggered slotted perforated channels, while Fig. 18 depicts the von Misses stress failure pattern for a 250 mm section depth solid and staggered slotted perforated channels. These figures highlight that staggered slotted perforations in the web, increases the sensitivity of the web buckling thus, decreases the ultimate local buckling bending capacity. In addition to that, deformation failure patterns obtained from the FE analysis for the staggered slotted perforated CFS channels are depicted in Fig. 19.

The parametric study results for the entire 432 models having staggered slotted perforations and corresponding solid web CFS channels results are presented in three tables; Table 5-7. Here, the aforementioned tables carry the results for the yield strengths of 300, 500, and 600

MPa, respectively. In these tables, M_{slots}, denotes the ultimate bending capacity of the staggered slotted perforated CFS beams prominently failed in local buckling while, M_{solid}, denotes the ultimate bending capacity of the corresponding solid CFS beams prominently failed in local buckling. Moreover, Tables 5-7 also present the M_{slots}/M_{soild} ratios (identified as reduction factor herein) and from this, the reduction of the bending capacity due to the staggered slotted perforations are examined.

Zhao et al. [16] found that a small ultimate bending capacity reduction occurs when cold-formed lipped channel beams with rectangular web openings predominantly fail under local buckling. Performing experimental studies they observed that the ultimate bending capacity reduction is approximately 16% when the rectangular opening height-to-web depth ratio is 0.8. Similarly, for staggered slotted perforated CFS channels, it was noticed that up to 11 % of bending capacity reduction was achieved and this has occurred when the web experiences the highest web area reduction. Further, a small reduction capacity was noticed when the web experiences the lowest web area reduction.

Table 5: Parametric study results for f_y = 300 MPa

No	Channels with Slotted Webs	M_{slots} (kNm)	M_{solid} (kNm)	M_{slots} / M_{solid}	No	Channels with Slotted Webs	M_{slots} (kNm)	M_{solid} (kNm)	M_{slots} / M_{solid}
1	150-1-60-3-1-6-300	3.11	3.17	0.98	73	250-1-60-3-1-6-300	5.54	5.55	1.00*
2	150-1-60-5-1-6-300	3.10	3.17	0.98	74	250-1-60-5-1-6-300	5.52	5.55	1.00*
3	150-1-75-3-1-6-300	3.11	3.17	0.98	75	250-1-75-3-1-6-300	5.53	5.55	1.00*
4	150-1-75-5-1-6-300	3.11	3.17	0.98	76	250-1-75-5-1-6-300	5.50	5.55	0.99
5	150-1-60-3-2-6-300	3.09	3.17	0.97	77	250-1-60-3-2-6-300	5.52	5.55	0.99
6	150-1-60-5-2-6-300	3.05	3.17	0.96	78	250-1-60-5-2-6-300	5.51	5.55	0.99
7	150-1-75-3-2-6-300	3.07	3.17	0.97	79	250-1-75-3-2-6-300	5.50	5.55	0.99
8	150-1-75-5-2-6-300	3.03	3.17	0.95	80	250-1-75-5-2-6-300	5.50	5.55	0.99
9	150-2-60-3-1-6-300	6.90	7.03	0.98	81	250-1-60-3-1-8-300	5.51	5.55	0.99
10	150-2-60-5-1-6-300	6.83	7.03	0.97	82	250-1-60-5-1-8-300	5.49	5.55	0.99
11	150-2-75-3-1-6-300	6.83	7.03	0.97	83	250-1-75-3-1-8-300	5.51	5.55	0.99
12	150-2-75-5-1-6-300	6.77	7.03	0.96	84	250-1-75-5-1-8-300	5.48	5.55	0.99
13	150-2-60-3-2-6-300	6.79	7.03	0.97	85	250-1-60-3-2-8-300	5.51	5.55	0.99
14	150-2-60-5-2-6-300	6.70	7.03	0.95	86	250-1-60-5-2-8-300	5.52	5.55	1.00*
15	150-2-75-3-2-6-300	6.74	7.03	0.96	87	250-1-75-3-2-8-300	5.50	5.55	0.99
16	150-2-75-5-2-6-300	6.63	7.03	0.94	88	250-1-75-5-2-8-300	5.48	5.55	0.99
17	150-3-60-3-1-6-300	10.13	10.40	0.97	89	250-1-60-3-1-12-300	5.48	5.55	0.99
18	150-3-60-5-1-6-300	10.05	10.40	0.97	90	250-1-60-5-1-12-300	5.46	5.55	0.98
19	150-3-75-3-1-6-300	10.39	10.40	1.00	91	250-1-75-3-1-12-300	5.46	5.55	0.98
20	150-3-75-5-1-6-300	10.31	10.40	0.99	92	250-1-75-5-1-12-300	5.47	5.55	0.99
21	150-3-60-3-2-6-300	10.05	10.40	0.97	93	250-1-60-3-2-12-300	5.47	5.55	0.99
22	150-3-60-5-2-6-300	9.86	10.40	0.95	94	250-1-60-5-2-12-300	5.45	5.55	0.98
23	150-3-75-3-2-6-300	10.29	10.40	0.99	95	250-1-75-3-2-12-300	5.43	5.55	0.98
24	150-3-75-5-2-6-300	10.08	10.40	0.97	96	250-1-75-5-2-12-300	5.41	5.55	0.98
25	200-1-60-3-1-6-300	4.28	4.34	0.99	97	250-2-60-3-1-6-300	15.89	16.30	0.97
26	200-1-60-5-1-6-300	4.27	4.34	0.98	98	250-2-60-5-1-6-300	15.79	16.30	0.97
27	200-1-75-3-1-6-300	4.25	4.34	0.98	99	250-2-75-3-1-6-300	15.69	16.30	0.96
28	200-1-75-5-1-6-300	4.24	4.34	0.98	100	250-2-75-5-1-6-300	15.58	16.30	0.96
29	200-1-60-3-2-6-300	4.26	4.34	0.98	101	250-2-60-3-2-6-300	15.76	16.30	0.97
30	200-1-60-5-2-6-300	4.23	4.34	0.97	102	250-2-60-5-2-6-300	15.67	16.30	0.96

31	200-1-75-3-2-6-300	4.23	4.34	0.97	103	250-2-75-3-2-6-300	15.52	16.30	0.95
32	200-1-75-5-2-6-300	4.19	4.34	0.97	104	250-2-75-5-2-6-300	15.40	16.30	0.95
33	200-1-60-3-1-8-300	4.25	4.34	0.98	105	250-2-60-3-1-8-300	15.74	16.30	0.97
34	200-1-60-5-1-8-300	4.25	4.34	0.98	106	250-2-60-5-1-8-300	15.64	16.30	0.96
35	200-1-75-3-1-8-300	4.23	4.34	0.97	107	250-2-75-3-1-8-300	15.50	16.30	0.95
36	200-1-75-5-1-8-300	4.20	4.34	0.97	108	250-2-75-5-1-8-300	15.38	16.30	0.94
37	200-1-60-3-2-8-300	4.21	4.34	0.97	109	250-2-60-3-2-8-300	15.57	16.30	0.96
38	200-1-60-5-2-8-300	4.20	4.34	0.97	110	250-2-60-5-2-8-300	15.47	16.30	0.95
39	200-1-75-3-2-8-300	4.20	4.34	0.97	111	250-2-75-3-2-8-300	15.52	16.30	0.95
40	200-1-75-5-2-8-300	4.18	4.34	0.96	112	250-2-75-5-2-8-300	15.20	16.30	0.93
41	200-2-60-3-1-6-300	10.20	10.22	1.00*	113	250-2-60-3-1-12-300	15.38	16.30	0.94
42	200-2-60-5-1-6-300	10.10	10.22	0.99	114	250-2-60-5-1-12-300	15.26	16.30	0.94
43	200-2-75-3-1-6-300	10.02	10.22	0.98	115	250-2-75-3-1-12-300	15.10	16.30	0.93
44	200-2-75-5-1-6-300	9.92	10.22	0.97	116	250-2-75-5-1-12-300	15.00	16.30	0.92
45	200-2-60-3-2-6-300	10.00	10.22	0.98	117	250-2-60-3-2-12-300	15.15	16.30	0.93
46	200-2-60-5-2-6-300	9.94	10.22	0.97	118	250-2-60-5-2-12-300	15.08	16.30	0.93
47	200-2-75-3-2-6-300	9.90	10.22	0.97	119	250-2-75-3-2-12-300	15.52	16.30	0.95
48	200-2-75-5-2-6-300	9.86	10.22	0.96	120	250-2-75-5-2-12-300	14.92	16.30	0.92
49	200-2-60-3-1-8-300	10.02	10.22	0.98	121	250-3-60-3-1-6-300	25.32	25.69	0.99
50	200-2-60-5-1-8-300	9.93	10.22	0.97	122	250-3-60-5-1-6-300	25.27	25.69	0.98
51	200-2-75-3-1-8-300	9.86	10.22	0.96	123	250-3-75-3-1-6-300	25.55	25.69	0.99
52	200-2-75-5-1-8-300	9.81	10.22	0.96	124	250-3-75-5-1-6-300	25.43	25.69	0.99
53	200-2-60-3-2-8-300	9.91	10.22	0.97	125	250-3-60-3-2-6-300	25.24	25.69	0.98
54	200-2-60-5-2-8-300	9.82	10.22	0.96	126	250-3-60-5-2-6-300	25.08	25.69	0.98
55	200-2-75-3-2-8-300	9.82	10.22	0.96	127	250-3-75-3-2-6-300	25.27	25.69	0.98
56	200-2-75-5-2-8-300	9.72	10.22	0.95	128	250-3-75-5-2-6-300	25.00	25.69	0.97
57	200-3-60-3-1-6-300	15.73	15.68	1.00*	129	250-3-60-3-1-8-300	25.45	25.69	0.99
58	200-3-60-5-1-6-300	15.64	15.68	1.00*	130	250-3-60-5-1-8-300	25.28	25.69	0.98
59	200-3-75-3-1-6-300	15.82	15.68	1.01*	131	250-3-75-3-1-8-300	25.22	25.69	0.98
60	200-3-75-5-1-6-300	15.73	15.68	1.00*	132	250-3-75-5-1-8-300	25.03	25.69	0.97
61	200-3-60-3-2-6-300	15.45	15.68	0.99	133	250-3-60-3-2-8-300	25.21	25.69	0.98
62	200-3-60-5-2-6-300	15.27	15.68	0.97	134	250-3-60-5-2-8-300	24.80	25.69	0.97
63	200-3-75-3-2-6-300	15.62	15.68	1.00*	135	250-3-75-3-2-8-300	24.94	25.69	0.97
64	200-3-75-5-2-6-300	15.42	15.68	0.98	136	250-3-75-5-2-8-300	24.66	25.69	0.96
65	200-3-60-3-1-8-300	15.48	15.68	0.99	137	250-3-60-3-1-12-300	24.72	25.69	0.96
66	200-3-60-5-1-8-300	15.35	15.68	0.98	138	250-3-60-5-1-12-300	24.45	25.69	0.95
67	200-3-75-3-1-8-300	15.59	15.68	0.99	139	250-3-75-3-1-12-300	24.71	25.69	0.96
68	200-3-75-5-1-8-300	15.51	15.68	0.99	140	250-3-75-5-1-12-300	24.44	25.69	0.95
69	200-3-60-3-2-8-300	15.25	15.68	0.97	141	250-3-60-3-2-12-300	24.32	25.69	0.95
70	200-3-60-5-2-8-300	14.98	15.68	0.96	142	250-3-60-5-2-12-300	23.92	25.69	0.93
71	200-3-75-3-2-8-300	15.41	15.68	0.98	143	250-3-75-3-2-12-300	24.35	25.69	0.95
72	200-3-75-5-2-8-300	15.08	15.68	0.96	144	250-3-75-5-2-12-300	23.93	25.69	0.93

Note: M_{slots} = bending capacity of slotted web channel, M_{solid} = bending capacity of solid web channel, * = numerical errors

Table 6: Parametric study results for f_y = 500 MPa

No	Channels with Slotted Webs	M_{slots} (kNm)	M_{solid} (kNm)	M_{slots} / M_{solid}	No	Channels with Slotted Webs	M_{slots} (kNm)	M_{solid} (kNm)	M_{slots} / M_{solid}
1	150-1-60-3-1-6-500	4.37	4.39	1.00*	73	250-1-60-3-1-6-500	7.27	7.33	0.99
2	150-1-60-5-1-6-500	4.39	4.39	1.00*	74	250-1-60-5-1-6-500	7.24	7.33	0.99
3	150-1-75-3-1-6-500	4.31	4.39	0.98	75	250-1-75-3-1-6-500	7.23	7.33	0.99
4	150-1-75-5-1-6-500	4.31	4.39	0.98	76	250-1-75-5-1-6-500	7.21	7.33	0.98
5	150-1-60-3-2-6-500	4.23	4.39	0.97	77	250-1-60-3-2-6-500	7.21	7.33	0.98
6	150-1-60-5-2-6-500	4.28	4.39	0.98	78	250-1-60-5-2-6-500	7.21	7.33	0.98
7	150-1-75-3-2-6-500	4.21	4.39	0.96	79	250-1-75-3-2-6-500	7.16	7.33	0.98
8	150-1-75-5-2-6-500	4.27	4.39	0.97	80	250-1-75-5-2-6-500	7.14	7.33	0.97
9	150-2-60-3-1-6-500	10.76	11.07	0.97	81	250-1-60-3-1-8-500	7.24	7.33	0.99
10	150-2-60-5-1-6-500	10.65	11.07	0.96	82	250-1-60-5-1-8-500	7.19	7.33	0.98
11	150-2-75-3-1-6-500	10.63	11.07	0.96	83	250-1-75-3-1-8-500	7.18	7.33	0.98
12	150-2-75-5-1-6-500	10.54	11.07	0.95	84	250-1-75-5-1-8-500	7.16	7.33	0.98

13	150-2-60-3-2-6-500	10.66	11.07	0.96	85	250-1-60-3-2-8-500	7.17	7.33	0.98
14	150-2-60-5-2-6-500	10.57	11.07	0.95	86	250-1-60-5-2-8-500	7.20	7.33	0.98
15	150-2-75-3-2-6-500	10.55	11.07	0.95	87	250-1-75-3-2-8-500	7.12	7.33	0.97
16	150-2-75-5-2-6-500	10.44	11.07	0.94	88	250-1-75-5-2-8-500	7.11	7.33	0.97
17	150-3-60-3-1-6-500	16.21	16.73	0.97	89	250-1-60-3-1-12-500	7.19	7.33	0.98
18	150-3-60-5-1-6-500	16.10	16.73	0.96	90	250-1-60-5-1-12-500	7.20	7.33	0.98
19	150-3-75-3-1-6-500	16.62	16.73	0.99	91	250-1-75-3-1-12-500	7.09	7.33	0.97
20	150-3-75-5-1-6-500	16.40	16.73	0.98	92	250-1-75-5-1-12-500	7.08	7.33	0.97
21	150-3-60-3-2-6-500	16.16	16.73	0.97	93	250-1-60-3-2-12-500	7.16	7.33	0.98
22	150-3-60-5-2-6-500	15.93	16.73	0.95	94	250-1-60-5-2-12-500	7.19	7.33	0.98
23	150-3-75-3-2-6-500	16.42	16.73	0.98	95	250-1-75-3-2-12-500	7.02	7.33	0.96
24	150-3-75-5-2-6-500	16.09	16.73	0.96	96	250-1-75-5-2-12-500	7.03	7.33	0.96
25	200-1-60-3-1-6-500	5.91	5.96	0.99	97	250-2-60-3-1-6-500	22.75	23.26	0.98
26	200-1-60-5-1-6-500	5.91	5.96	0.99	98	250-2-60-5-1-6-500	22.60	23.26	0.97
27	200-1-75-3-1-6-500	5.98	5.96	1.00*	99	250-2-75-3-1-6-500	22.48	23.26	0.97
28	200-1-75-5-1-6-500	5.94	5.96	1.00*	100	250-2-75-5-1-6-500	22.31	23.26	0.96
29	200-1-60-3-2-6-500	6.03	5.96	1.01*	101	250-2-60-3-2-6-500	22.48	23.26	0.97
30	200-1-60-5-2-6-500	6.01	5.96	1.01*	102	250-2-60-5-2-6-500	22.35	23.26	0.96
31	200-1-75-3-2-6-500	5.98	5.96	1.00*	103	250-2-75-3-2-6-500	22.19	23.26	0.95
32	200-1-75-5-2-6-500	5.92	5.96	0.99	104	250-2-75-5-2-6-500	22.00	23.26	0.95
33	200-1-60-3-1-8-500	6.00	5.96	1.01*	105	250-2-60-3-1-8-500	22.48	23.26	0.97
34	200-1-60-5-1-8-500	5.97	5.96	1.00*	106	250-2-60-5-1-8-500	22.34	23.26	0.96
35	200-1-75-3-1-8-500	5.89	5.96	0.99	107	250-2-75-3-1-8-500	22.19	23.26	0.95
36	200-1-75-5-1-8-500	5.83	5.96	0.98	108	250-2-75-5-1-8-500	22.02	23.26	0.95
37	200-1-60-3-2-8-500	5.90	5.96	0.99	109	250-2-60-3-2-8-500	22.20	23.26	0.95
38	200-1-60-5-2-8-500	5.90	5.96	0.99	110	250-2-60-5-2-8-500	22.07	23.26	0.95
39	200-1-75-3-2-8-500	5.92	5.96	0.99	111	250-2-75-3-2-8-500	21.86	23.26	0.94
40	200-1-75-5-2-8-500	5.87	5.96	0.98	112	250-2-75-5-2-8-500	21.66	23.26	0.93
41	200-2-60-3-1-6-500	15.48	15.60	0.99	113	250-2-60-3-1-12-500	21.93	23.26	0.94
42	200-2-60-5-1-6-500	15.35	15.60	0.98	114	250-2-60-5-1-12-500	21.75	23.26	0.94
43	200-2-75-3-1-6-500	15.07	15.60	0.97	115	250-2-75-3-1-12-500	21.53	23.26	0.93
44	200-2-75-5-1-6-500	14.92	15.60	0.96	116	250-2-75-5-1-12-500	21.34	23.26	0.92
45	200-2-60-3-2-6-500	15.08	15.60	0.97	117	250-2-60-3-2-12-500	21.43	23.26	0.92
46	200-2-60-5-2-6-500	15.02	15.60	0.96	118	250-2-60-5-2-12-500	21.28	23.26	0.91
47	200-2-75-3-2-6-500	14.77	15.60	0.95	119	250-2-75-3-2-12-500	21.02	23.26	0.90
48	200-2-75-5-2-6-500	14.79	15.60	0.95	120	250-2-75-5-2-12-500	20.88	23.26	0.90
49	200-2-60-3-1-8-500	15.08	15.60	0.97	121	250-3-60-3-1-6-500	38.72	39.64	0.98
50	200-2-60-5-1-8-500	14.93	15.60	0.96	122	250-3-60-5-1-6-500	38.55	39.64	0.97
51	200-2-75-3-1-8-500	14.65	15.60	0.94	123	250-3-75-3-1-6-500	38.89	39.64	0.98
52	200-2-75-5-1-8-500	14.52	15.60	0.93	124	250-3-75-5-1-6-500	38.65	39.64	0.98
53	200-2-60-3-2-8-500	15.00	15.60	0.96	125	250-3-60-3-2-6-500	38.53	39.64	0.97
54	200-2-60-5-2-8-500	14.93	15.60	0.96	126	250-3-60-5-2-6-500	38.27	39.64	0.97
55	200-2-75-3-2-8-500	14.72	15.60	0.94	127	250-3-75-3-2-6-500	38.45	39.64	0.97
56	200-2-75-5-2-8-500	14.73	15.60	0.94	128	250-3-75-5-2-6-500	38.12	39.64	0.96
57	200-3-60-3-1-6-500	24.52	24.72	0.99	129	250-3-60-3-1-8-500	38.54	39.64	0.97
58	200-3-60-5-1-6-500	24.37	24.72	0.99	130	250-3-60-5-1-8-500	38.22	39.64	0.96
59	200-3-75-3-1-6-500	24.60	24.72	1.00*	131	250-3-75-3-1-8-500	38.43	39.64	0.97
60	200-3-75-5-1-6-500	24.45	24.72	0.99	132	250-3-75-5-1-8-500	38.10	39.64	0.96
61	200-3-60-3-2-6-500	24.22	24.72	0.98	133	250-3-60-3-2-8-500	38.10	39.64	0.96
62	200-3-60-5-2-6-500	24.06	24.72	0.97	134	250-3-60-5-2-8-500	37.78	39.64	0.95
63	200-3-75-3-2-6-500	24.46	24.72	0.99	135	250-3-75-3-2-8-500	37.93	39.64	0.96
64	200-3-75-5-2-6-500	24.25	24.72	0.98	136	250-3-75-5-2-8-500	37.57	39.64	0.95
65	200-3-60-3-1-8-500	24.19	24.72	0.98	137	250-3-60-3-1-12-500	37.66	39.64	0.95
66	200-3-60-5-1-8-500	24.03	24.72	0.97	138	250-3-60-5-1-12-500	37.27	39.64	0.94
67	200-3-75-3-1-8-500	24.30	24.72	0.98	139	250-3-75-3-1-12-500	37.45	39.64	0.94
68	200-3-75-5-1-8-500	24.16	24.72	0.98	140	250-3-75-5-1-12-500	37.10	39.64	0.94
69	200-3-60-3-2-8-500	23.90	24.72	0.97	141	250-3-60-3-2-12-500	37.04	39.64	0.93
70	200-3-60-5-2-8-500	23.69	24.72	0.96	142	250-3-60-5-2-12-500	36.67	39.64	0.93
71	200-3-75-3-2-8-500	24.13	24.72	0.98	143	250-3-75-3-2-12-500	36.98	39.64	0.93

72	200-3-75-5-2-8-500	23.77	24.72	0.96	144	250-3-75-5-2-12-500	36.68	39.64	0.93

328 Note: M_{slots} = bending capacity of slotted web channel, M_{solid} = bending capacity of solid web channel, * = numerical errors

329

330 Table 7: Parametric study results for f_y = 600 MPa

No	Channels with Slotted Webs	M_{slots} (kNm)	M_{solid} (kNm)	M_{slots} / M_{solid}	No	Channels with Slotted Webs	M_{slots} (kNm)	M_{solid} (kNm)	M_{slots} / M_{solid}
1	150-1-60-3-1-6-600	4.69	4.79	0.98	73	250-1-60-3-1-6-600	8.04	8.09	0.99
2	150-1-60-5-1-6-600	4.69	4.79	0.98	74	250-1-60-5-1-6-600	8.02	8.09	0.99
3	150-1-75-3-1-6-600	4.65	4.79	0.97	75	250-1-75-3-1-6-600	8.00	8.09	0.99
4	150-1-75-5-1-6-600	4.66	4.79	0.97	76	250-1-75-5-1-6-600	7.97	8.09	0.98
5	150-1-60-3-2-6-600	4.64	4.79	0.97	77	250-1-60-3-2-6-600	7.89	8.09	0.97
6	150-1-60-5-2-6-600	4.70	4.79	0.98	78	250-1-60-5-2-6-600	7.90	8.09	0.98
7	150-1-75-3-2-6-600	4.60	4.79	0.96	79	250-1-75-3-2-6-600	7.88	8.09	0.97
8	150-1-75-5-2-6-600	4.69	4.79	0.98	80	250-1-75-5-2-6-600	7.86	8.09	0.97
9	150-2-60-3-1-6-600	12.51	12.94	0.97	81	250-1-60-3-1-8-600	8.02	8.09	0.99
10	150-2-60-5-1-6-600	12.39	12.94	0.96	82	250-1-60-5-1-8-600	7.94	8.09	0.98
11	150-2-75-3-1-6-600	12.38	12.94	0.96	83	250-1-75-3-1-8-600	7.91	8.09	0.98
12	150-2-75-5-1-6-600	12.26	12.94	0.95	84	250-1-75-5-1-8-600	7.89	8.09	0.98
13	150-2-60-3-2-6-600	12.46	12.94	0.96	85	250-1-60-3-2-8-600	7.87	8.09	0.97
14	150-2-60-5-2-6-600	12.37	12.94	0.96	86	250-1-60-5-2-8-600	7.89	8.09	0.98
15	150-2-75-3-2-6-600	12.31	12.94	0.95	87	250-1-75-3-2-8-600	7.85	8.09	0.97
16	150-2-75-5-2-6-600	12.20	12.94	0.94	88	250-1-75-5-2-8-600	7.82	8.09	0.97
17	150-3-60-3-1-6-600	19.07	19.66	0.97	89	250-1-60-3-1-12-600	7.90	8.09	0.98
18	150-3-60-5-1-6-600	18.97	19.66	0.96	90	250-1-60-5-1-12-600	7.84	8.09	0.97
19	150-3-75-3-1-6-600	19.53	19.66	0.99	91	250-1-75-3-1-12-600	7.79	8.09	0.96
20	150-3-75-5-1-6-600	19.22	19.66	0.98	92	250-1-75-5-1-12-600	7.78	8.09	0.96
21	150-3-60-3-2-6-600	19.04	19.66	0.97	93	250-1-60-3-2-12-600	7.86	8.09	0.97
22	150-3-60-5-2-6-600	18.79	19.66	0.96	94	250-1-60-5-2-12-600	7.92	8.09	0.98
23	150-3-75-3-2-6-600	19.24	19.66	0.98	95	250-1-75-3-2-12-600	7.74	8.09	0.96
24	150-3-75-5-2-6-600	18.88	19.66	0.96	96	250-1-75-5-2-12-600	7.72	8.09	0.95
25	200-1-60-3-1-6-600	6.47	6.52	0.99	97	250-2-60-3-1-6-600	25.16	26.02	0.97
26	200-1-60-5-1-6-600	6.45	6.52	0.99	98	250-2-60-5-1-6-600	25.02	26.02	0.96
27	200-1-75-3-1-6-600	6.39	6.52	0.98	99	250-2-75-3-1-6-600	24.94	26.02	0.96
28	200-1-75-5-1-6-600	6.35	6.52	0.97	100	250-2-75-5-1-6-600	24.77	26.02	0.95
29	200-1-60-3-2-6-600	6.37	6.52	0.98	101	250-2-60-3-2-6-600	24.93	26.02	0.96
30	200-1-60-5-2-6-600	6.37	6.52	0.98	102	250-2-60-5-2-6-600	24.81	26.02	0.95
31	200-1-75-3-2-6-600	6.35	6.52	0.97	103	250-2-75-3-2-6-600	24.68	26.02	0.95
32	200-1-75-5-2-6-600	6.33	6.52	0.97	104	250-2-75-5-2-6-600	24.49	26.02	0.94
33	200-1-60-3-1-8-600	6.39	6.52	0.98	105	250-2-60-3-1-8-600	24.93	26.02	0.96
34	200-1-60-5-1-8-600	6.35	6.52	0.97	106	250-2-60-5-1-8-600	24.80	26.02	0.95
35	200-1-75-3-1-8-600	6.36	6.52	0.98	107	250-2-75-3-1-8-600	24.68	26.02	0.95
36	200-1-75-5-1-8-600	6.34	6.52	0.97	108	250-2-75-5-1-8-600	24.50	26.02	0.94
37	200-1-60-3-2-8-600	6.33	6.52	0.97	109	250-2-60-3-2-8-600	24.70	26.02	0.95
38	200-1-60-5-2-8-600	6.29	6.52	0.96	110	250-2-60-5-2-8-600	24.53	26.02	0.94
39	200-1-75-3-2-8-600	6.40	6.52	0.98	111	250-2-75-3-2-8-600	24.35	26.02	0.94
40	200-1-75-5-2-8-600	6.27	6.52	0.96	112	250-2-75-5-2-8-600	24.13	26.02	0.93
41	200-2-60-3-1-6-600	17.74	17.99	0.99	113	250-2-60-3-1-12-600	24.40	26.02	0.94
42	200-2-60-5-1-6-600	17.67	17.99	0.98	114	250-2-60-5-1-12-600	24.22	26.02	0.93
43	200-2-75-3-1-6-600	17.25	17.99	0.96	115	250-2-75-3-1-12-600	24.02	26.02	0.92
44	200-2-75-5-1-6-600	17.07	17.99	0.95	116	250-2-75-5-1-12-600	23.80	26.02	0.91
45	200-2-60-3-2-6-600	17.20	17.99	0.96	117	250-2-60-3-2-12-600	23.83	26.02	0.92
46	200-2-60-5-2-6-600	17.10	17.99	0.95	118	250-2-60-5-2-12-600	23.61	26.02	0.91
47	200-2-75-3-2-6-600	16.74	17.99	0.93	119	250-2-75-3-2-12-600	23.35	26.02	0.90
48	200-2-75-5-2-6-600	16.70	17.99	0.93	120	250-2-75-5-2-12-600	23.11	26.02	0.89
49	200-2-60-3-1-8-600	17.16	17.99	0.95	121	250-3-60-3-1-6-600	44.29	45.46	0.97
50	200-2-60-5-1-8-600	16.98	17.99	0.94	122	250-3-60-5-1-6-600	44.08	45.46	0.97
51	200-2-75-3-1-8-600	16.68	17.99	0.93	123	250-3-75-3-1-6-600	44.47	45.46	0.98

52	200-2-75-5-1-8-600	16.53	17.99	0.92	124	250-3-75-5-1-6-600	44.18	45.46	0.97
53	200-2-60-3-2-8-600	17.12	17.99	0.95	125	250-3-60-3-2-6-600	44.06	45.46	0.97
54	200-2-60-5-2-8-600	17.15	17.99	0.95	126	250-3-60-5-2-6-600	43.74	45.46	0.96
55	200-2-75-3-2-8-600	16.74	17.99	0.93	127	250-3-75-3-2-6-600	43.89	45.46	0.97
56	200-2-75-5-2-8-600	16.82	17.99	0.93	128	250-3-75-5-2-6-600	43.47	45.46	0.96
57	200-3-60-3-1-6-600	28.55	28.84	0.99	129	250-3-60-3-1-8-600	44.05	45.46	0.97
58	200-3-60-5-1-6-600	28.37	28.84	0.98	130	250-3-60-5-1-8-600	43.67	45.46	0.96
59	200-3-75-3-1-6-600	28.61	28.84	0.99	131	250-3-75-3-1-8-600	43.89	45.46	0.97
60	200-3-75-5-1-6-600	28.41	28.84	0.99	132	250-3-75-5-1-8-600	43.47	45.46	0.96
61	200-3-60-3-2-6-600	28.22	28.84	0.98	133	250-3-60-3-2-8-600	43.50	45.46	0.96
62	200-3-60-5-2-6-600	28.07	28.84	0.97	134	250-3-60-5-2-8-600	43.11	45.46	0.95
63	200-3-75-3-2-6-600	28.50	28.84	0.99	135	250-3-75-3-2-8-600	43.22	45.46	0.95
64	200-3-75-5-2-6-600	28.28	28.84	0.98	136	250-3-75-5-2-8-600	42.79	45.46	0.94
65	200-3-60-3-1-8-600	28.15	28.84	0.98	137	250-3-60-3-1-12-600	42.94	45.46	0.94
66	200-3-60-5-1-8-600	27.98	28.84	0.97	138	250-3-60-5-1-12-600	42.47	45.46	0.93
67	200-3-75-3-1-8-600	28.24	28.84	0.98	139	250-3-75-3-1-12-600	42.59	45.46	0.94
68	200-3-75-5-1-8-600	28.08	28.84	0.97	140	250-3-75-5-1-12-600	42.18	45.46	0.93
69	200-3-60-3-2-8-600	27.85	28.84	0.97	141	250-3-60-3-2-12-600	42.14	45.46	0.93
70	200-3-60-5-2-8-600	27.69	28.84	0.96	142	250-3-60-5-2-12-600	41.79	45.46	0.92
71	200-3-75-3-2-8-600	28.13	28.84	0.98	143	250-3-75-3-2-12-600	41.97	45.46	0.92
72	200-3-75-5-2-8-600	27.77	28.84	0.96	144	250-3-75-5-2-12-600	41.73	45.46	0.92

Note: M_{slots} = bending capacity of slotted web channel, M_{solid} = bending capacity of solid web channel

The variation of the reduction factors against the considered parameters is plotted in Fig. 20. It can be noted that the reduction factor is higher when the number of slot row groups, N =2 compare to N=1. In the case of N=1, the slotted perforations are placed near the neutral axis while in the case of N=2, slotted perforations are moved towards the web-flange junction. Therefore, when N=2, the staggered slotted perforations are subjected to high compressive stress and thus lead to higher bending capacity reduction. Overall, from Fig. 20, it can be observed that when the total number of slot rows (n), slot length (L_{sl}), and slot width (W_{sl}) increases the staggered slotted perforated CFS beams led higher bending capacity reduction. This is due to removal of high web area when these parameters increases. Moreover, Fig. 20 also illustrates the variation of the reduction factor against the yield strength. High reduction in the bending capacity is observed with the yield strength.

5 Extended DSM based design method for slotted perforated beams

5.1 General

The DSM is a convenient method to design CFS members. It predicts the ultimate load carrying capacity of the CFS structural member based on its elastic and yield capacities. The advanced FE modelling techniques boost the DSM, as the elastic and yielding capacities can be easily determined from FE analysis. Therefore, the use of conventional effective width method available in standards design codes is decreasing, however, it is still being used for verification and comparison purposes. The DSM has been adopted in North American specification for the

design of cold-formed structural members, NAS AISI S100 [25], and Australian and New Zealand standard for cold-formed steel structures, AS/NZ 4600 [26]. However this design method is still not included into the Eurocode (EN1993-1-3 [27]). Initially, DSM design was developed for CFS solid web beams and in addition, the latest version of the NAS AISI S100 [25] and AS/NZ 4600 [26] carries the extended version for the DSM of CFS beams with openings subject to local and distortional buckling. Since this paper focuses on the local buckling behaviour of slotted perforated CFS beams, following sections explains the available DSM provisions and the proposed extended version to accommodate the staggered slotted perforations.

5.2 Direct strength method for solid web CFS beams

As discussed in the previous section, the ultimate bending capacity of a CFS solid web channel subject to local buckling is determined from section F3.2.1 of NAS AISI S100 [25] and clause 7.2.2.3.2 of AS/NZ 4600 [26]. The ultimate bending capacity for local buckling (M_{bl}) of the solid web CFS channels can be determined from Eqs. 1 and 2.

For $\lambda_l \leq 0.776$, $$M_{bl} = M_{be} \quad (1)$$

For $\lambda_l > 0.776$, $$M_{bl} = \left[1 - 0.15\left(\frac{M_{ol}}{M_{be}}\right)^{0.4}\right]\left(\frac{M_{ol}}{M_{be}}\right)^{0.4} M_{be} \quad (2)$$

Where $\lambda_l = \sqrt{M_{be}/M_{ol}}$, λ_l is the non-dimensional slenderness to calculate M_{bl}, and M_{be} is the nominal member moment capacity for lateral torsional buckling of the CFS section. This M_{be} is replaced with the yielding moment, M_y, which is the product of the elastic section modulus (Z) of the section and yield strength when the lateral-torsional buckling is prevented through lateral braces. M_{ol} is the elastic local buckling moment.

In addition, both NAS AISI S100 [25] and AS/NZ 4600 [26] carries the modified version of Eq. 1, accounting the inelastic reserve capacity for the local buckling of CFS beams, which experience higher compressive strain. The inelastic reserve capacity is permitted when $M_{be} > M_y$ and $\lambda_l \leq 0.776$. Therefore, the inelastic reserve capacity under the category of CFS sections symmetric about the axis of bending or sections with first yield in compression can be determined using Eq. 3.

For $\lambda_l \leq 0.776$, $$M_{bl} = M_y + \left[1 - \frac{1}{C_{yd}^2}\right](M_p - M_y) \quad (3)$$

Where M_p denotes the plastic moment, which is the product of plastic section modulus (S) and yield strength (f_y) and $c_{yd} = \sqrt{0.776/\lambda_l} \leq 3$.

The ultimate bending capacity prediction of solid CFS beams subject to local buckling using current DSM equations is plotted in Fig. 21. It is noteworthy to mention that the plastic moment (M_p), is required to plot the inelastic reserve in the DSM plot. Therefore, the solid CFS beams were analysed to calculate the elastic section modulus (Z) and plastic section modulus (S) of the solid CFS sections. From this, the shape factor (S/Z) was obtained which is equal to the $M_p\,/M_y$ ratio. Table 4 contains the shape factor values and the mean shape factor value of 1.26. In concern to the conservative approach the minimum shape factor 1.21 was chosen over the mean value. Fig. 22 shows the FE capacity predictions for the solid CFS beams. These predictions show a satisfactory agreement with the DSM predictions.

5.3 Direct strength method for CFS beams with holes.

The DSM design provision for CFS beams with web holes is provided in Australian/New Zealand Standard AS/NZS 4600 [26] and North American Specification NAS AISI S100 [25], although the previous versions do not have provisions for web holes. Clause F3.2.2 of NAS AISI S100 [25] and section 7.2.2.3.3 of AS/NZ 4600 [26] suggest that the ultimate flexural strength of CFS beams with web openings can be determined using the DSM equations for solid web CFS beams (Eq. 1 and 2). However, M_{ol} needs to be calculated with the influence of web holes and $M_{bl} \leq M_{ynet}$. Here, M_{ynet} is the yield moment of the net cross-section. This can be summarised as follows:

For $\lambda_l \leq 0.776$, $\quad M_{bl} = M_{ynet}$ (4)

For $\lambda_l > 0.776$, $\quad M_{bl} = \left[1 - 0.15\left(\frac{M_{ol}}{M_{be}}\right)^{0.4}\right]\left(\frac{M_{ol}}{M_{be}}\right)^{0.4} M_{be} \leq M_{ynet}$ (5)

Here M_{be} can be replaced with M_y for laterally braced beams. The DSM curve for local buckling accounting web holes varies based on the $M_{ynet}\,/M_y$ ratio, which defines the size of the web holes with respect to the full web height. The DSM curve for local buckling considering the effect of web hole is plotted in Fig. 23 considering a typical value of 0.85 for $M_{ynet}\,/M_y$.

5.4 New DSM based design equations for slotted perforated channels

As discussed in section 5.3, NAS AISI S100 [25] and AS/NZ 4600 [26] provide DSM based design predictions for CFS beams with web holes. However, DSM based design equations are no longer accurate and cannot account for the new generation of slot configurations. A series of staggered slotted perforations are located vertically and horizontally in staggered slotted

perforated CFS beams in comparison to conventional discrete holes. Therefore, the DSM needs to be modified to account the effect of staggered slotted perforations. This can be achieved through modifying the local buckling moment, M_{ol}, and yield moment, M_y. However, this would make the DSM equations for local buckling more complex alike, the DSM equations for CFS beams with web holes to predict the distortional buckling capacity. Hence, a simple approach is to develop a reduction factor (q_s) in terms of the influencing dimensional and mechanical parameters on the flexural capacity. These influencing parameters have been focused in the parametric study. Using this concept, the ultimate bending capacity of the staggered slotted CFS beams subject to local buckling (M_{slots}) can be determined through applying the reduction factor (q_s) to its corresponding bending capacity of the solid CFS beams subject to local buckling (M_{solid}). This can be written as follows:

$$M_{slots} = M_{solid} \times q_s \tag{6}$$

The reduction factor, q_s, was proposed based on the ultimate bending capacity results of 432 FE models which were generated for the parametric study. It was aimed to develop this factor as a function of the influencing parameters considered in the parametric study. The influencing parameters are section depth (D), flange width (B_f), lip length (B_l), thickness (t), slot length (L_{sl}), slot width (W_{sl}), total number of slot rows (n), number of slot row groups (N) and yield strength (f_y). The local buckling strength of the CFS beam is majorly governed by the slenderness of the web, flange, and lip segments. Therefore, the slenderness of each segments (D/t), (B_f/t), and (B_l/t) were considered in the equation. The dimensional parameters of the staggered slotted perforations were considered as normalised ratios with respect to their limiting dimensions. The slot length (L_{sl}) and slot width (W_{sl}) were normalised with 100 mm and 9.5 mm, respectively while the number of slot row groups (N) is normalised with the total number of slot rows (n). Similarly, the yield strength (f_y) was normalised with 250 MPa. The proposed equation for the reduction factor is as follows:

$$q_s = 1 - \frac{\left[\frac{B_f}{t}\right]^{2.683}\left[\frac{L_{sl}}{100}\right]^{0.891}\left[\frac{W_{sl}}{9.5}\right]^{0.490}\left[\frac{f_y}{250}\right]^{0.368}}{\left[\frac{D}{t}\right]^{2.132}\left[\frac{B_l}{t}\right]^{0.998}\left[\frac{N}{n}\right]^{0.076}} \tag{7}$$

The classic genetic algorithm and Generalised Reduced Gradient (GRG) solving method were used to develop and optimise the equation. During the optimisation, the objective function was set such that the mean for the q_s(FE)/q_s(proposed) ratios of 432 models equal to unity, while maintaining the COV value as minimal as possible. This optimisation mechanism resulted in accurate power values of the considered influencing parameters on local buckling capacity.The

optimisation resulted in a COV value of 0.019. This shows a high accuracy of the proposed reduction factor equation. An illustration of the accuracy of the proposed reduction factor is provided in Fig. 24 for the yield strengths of 300, 500, and 600 MPa separately.

Therefore, the proposed reduction factor (q_s) can be adopted into the DSM equations for solid CFS beams subject to local buckling to convert them as accounting for the staggered slotted perforations. Eqs. 8 and 9 present the new DSM based design equations to predict the ultimate bending capacity of the staggered slotted perforated CFS beams subject to local buckling.

For $\lambda_l \leq 0.776$, $$M_{bl,slots} = \left\{M_y + \left[1 - \frac{1}{C_{yd}^2}\right]\left(M_p - M_y\right)\right\} q_s \quad (8)$$

For $\lambda_l > 0.776$, $$M_{bl,slots} = \left\{\left[1 - 0.15\left(\frac{M_{ol}}{M_y}\right)^{0.4}\right]\left(\frac{M_{ol}}{M_{y,}}\right)^{0.4} M_y\right\} q_s \quad (9)$$

Here q_s is substituted from Eq. 7.

The ultimate bending capacity predictions for the staggered slotted perforated CFS beams for the 432 FE models are plotted with DSM curve for local buckling in Fig. 25. It illustrates that DSM equation curves give the lower bounds of the predicted results for the staggered slotted perforated CFS beams. Therfeore, the proposed new DSM based equations can be employed for resasonable and conservative predictions for the new generations of slotted perforated CFS beams subject to local buckling.

6 Conclusions

The new generation CFS beam with staggered slotted perforations is becoming popular due to the amplified thermal performance. However, these web perforations affect the bending capacity. Therefore, the bending capacity of the CFS beams with staggered slotted perforations subject to local buckling were analysed by FE models in ANSYS. FE models were developed and validated against experimental results in terms of failure modes and moment capacities. The validated FE models were used to conduct a comprehensive parametric study of 432 FE models varying the dimensional and mechanical parameters of the slotted perforated CFS beams. It was found that the influence of staggered slotted perforations on local buckling strength of the CFS beams is relatively small, with a maximum reduction value of 11 %. Furthermore, the ultimate bending capacity results obtained from FE parametric analyses were used to develop new DSM based design equations for CFS beams with staggered slotted perforations subject to local buckling. The new DSM for local buckling has shown a good

agreement with the FE results. Therefore, the proposed equations will enhance the commercial aspects of the new generation of staggered slotted CFS beams.

Acknowledgements

The authors would like to appreciate the necessary research facilities such as the super computer resources from South Ural State University and technical assistance from Northumbria University.

References

[1] T. Hoglund, H. Burstand b, Slotted steel studs to reduce thermal bridges in insulated walls, Thin-Walled Structures 32(1-3) (1998) 81-109.
[2] R. LaBoube, Development of cost-effective, energy efficient steel framing: Thermal performance of slit-web steel wall studs, 2006.
[3] J. Lipták-Váradi, Equivalent thermal conductivity of steel girders with slotted web, Periodica Polytechnica Civil Engineering 54(2) (2010).
[4] F. Liu, F. Fu, Y. Wang, Q. Liu, Fire performance of non-load-bearing light-gauge slotted steel stud walls, Journal of Constructional Steel Research 137 (2017) 228-241.
[5] J. Kesti, Local and distortional buckling of perforated steel wall studs, Helsinki University of Technology, 2000.
[6] V.V. Degtyarev, N.V. Degtyareva, Finite element modeling of cold-formed steel channels with solid and slotted webs in shear, Thin-Walled Structures 103 (2016) 183-198.
[7] N.V. Degtyareva, V.V. Degtyarev, Experimental investigation of cold-formed steel channels with slotted webs in shear, Thin-Walled Structures 102 (2016) 30-42.
[8] N. Degtyareva, P. Gatheeshgar, K. Poologanathan, S. Gunalan, M. Lawson, P. Sunday, Combined bending and shear behaviour of slotted perforated steel channels: Numerical studies, Journal of Constructional Steel Research 161 (2019) 369-384.
[9] C. Yu, B.W. Schafer, Distortional buckling test on cold-formed steel beams, Journal of Structural Fire Engineering 132(4) (2006) 515-528.
[10] C. Yu, B.W. Shafer, Local buckling test on cold-formed steel beams, Journal of Structural Engineering 129(12) (2003) 1596-1606.
[11] C.H. Pham, G.J. Hancock, Experimental Investigation and Direct Strength Design of High-Strength, Complex C-Sections in Pure Bending, Journal of Structural Engineering 139(11) (2013) 1842-1852.
[12] R. Siahaan, P. Keerthan, M. Mahendran, Section moment capacity design rules for rivet fastened rectangular hollow flange channel beams, Thin-Walled Structures 127 (2018) 781-797.
[13] R. Siahaan, P. Keerthan, M. Mahendran, Finite element modeling of rivet fastened rectangular hollow flange channel beams subject to local buckling, Engineering Structures 126 (2016) 311-327.
[14] R. Siahaan, M. Mahendran, P. Keerthan, Section moment capacity tests of rivet fastened rectangular hollow flange channel beams, Journal of Constructional Steel Research 125 (2016) 252-262.
[15] C.D. Moen, A. Schudlich, A. von der Heyden, Experiments on Cold-Formed Steel C-Section Joists with Unstiffened Web Holes, Journal of Structural Engineering 139(5) (2013) 695-704.
[16] J. Zhao, K. Sun, C. Yu, J. Wang, Tests and direct strength design on cold-formed steel channel beams with web holes, Engineering Structures 184 (2019) 434-446.
[17] N. Yu, B. Kim, L. Li, W. Hong, W. Yuan, Distortional buckling of perforated cold-formed steel beams subject to uniformly distributed transverse loads, Thin-Walled Structures 148 (2020).

[18] N. Yu, B. Kim, W. Yuan, L. Li, F. Yu, An analytical solution of distortional buckling resistance of cold-formed steel channel-section beams with web openings, Thin-Walled Structures 135 (2019) 446-452.
[19] N.V. Degtyarev, Review of experimental studies of cold-formed steel channels with slotted webs under bending, Procedia Engineering 206 (2017) 875-880.
[20] ANSYS, Commands reference, elements reference, operations guide, Basic Analysis Guide, Theory Reference for ANSYS, 2019.
[21] B.W. Schafer, T. Pekoz, Computational modeling of cold-formed steel: characterizing geometric imperfections and residual stresses, Journal of Constructional Steel Research 47 (1998) 193-210.
[22] M.R. Haidarali, D.A. Nethercot, Finite element modelling of cold-formed steel beams under local buckling or combined local/distortional buckling, Thin-Walled Structures 49(12) (2011) 1554-1562.
[23] B.W. Schafer, Z. Li, C.D. Moen, Computational modeling of cold-formed steel, Thin-Walled Structures 48(10-11) (2010) 752-762.
[24] C.H. Pham, G.J. Hancock, Numerical simulation of high strength cold-formed purlins in combined bending and shear, Journal of Constructional Steel Research 66(10) (2010) 1205-1217.
[25] North American Specification for the Design of Cold-Formed Steel Structural Members, American Iron and Steel Institute, 2016.
[26] Australian/New Zealand Standard AS/NZ 4600, Cold-formed steel structures, Sydney, Australia, 2018.
[27] CEN, Eurocode 3 - Design of steel structures - Part 1-3 General rules- Supplementary rules for cold-formed members and sheeting, European Comittee for Standardization, Brussels, 2006.

Fig. 1. Application of slotted perforated CFS beams as floor joists

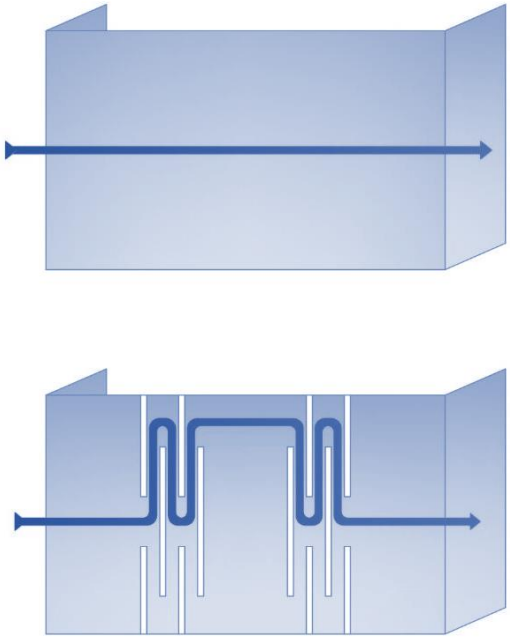

Fig. 2. Heat transmittance path in solid and slotted web CFS beams

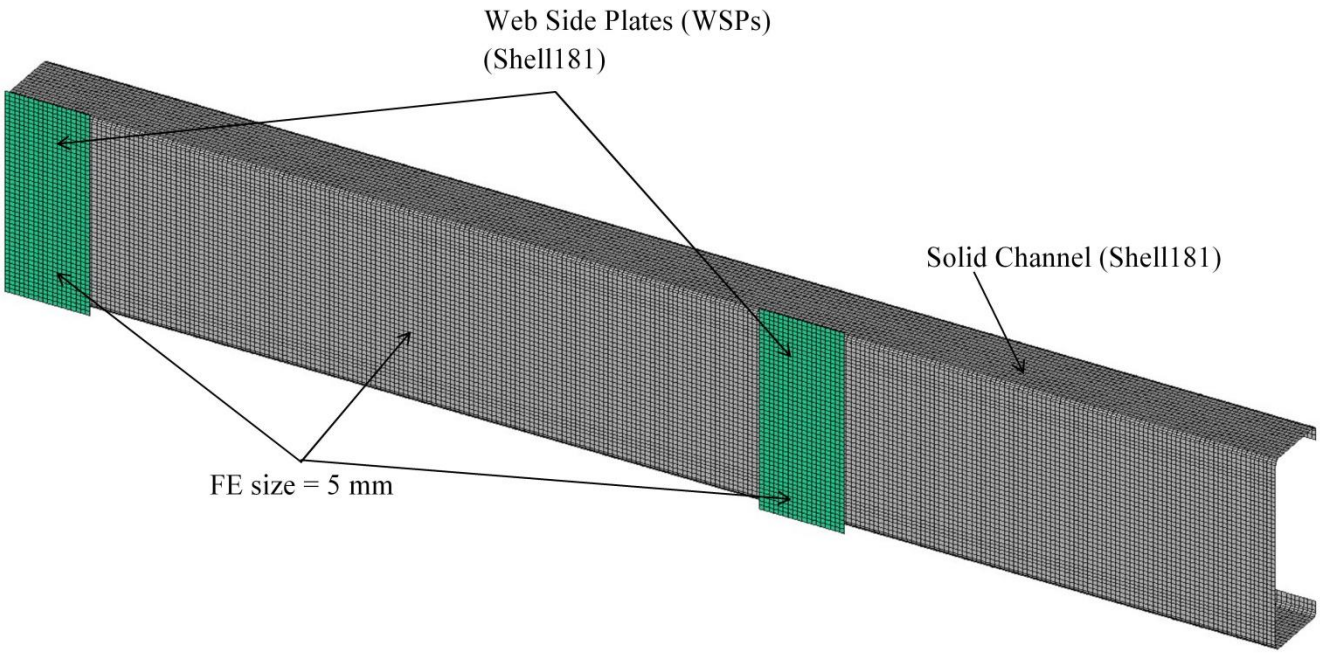

Fig. 3. Assigned element type and mesh size

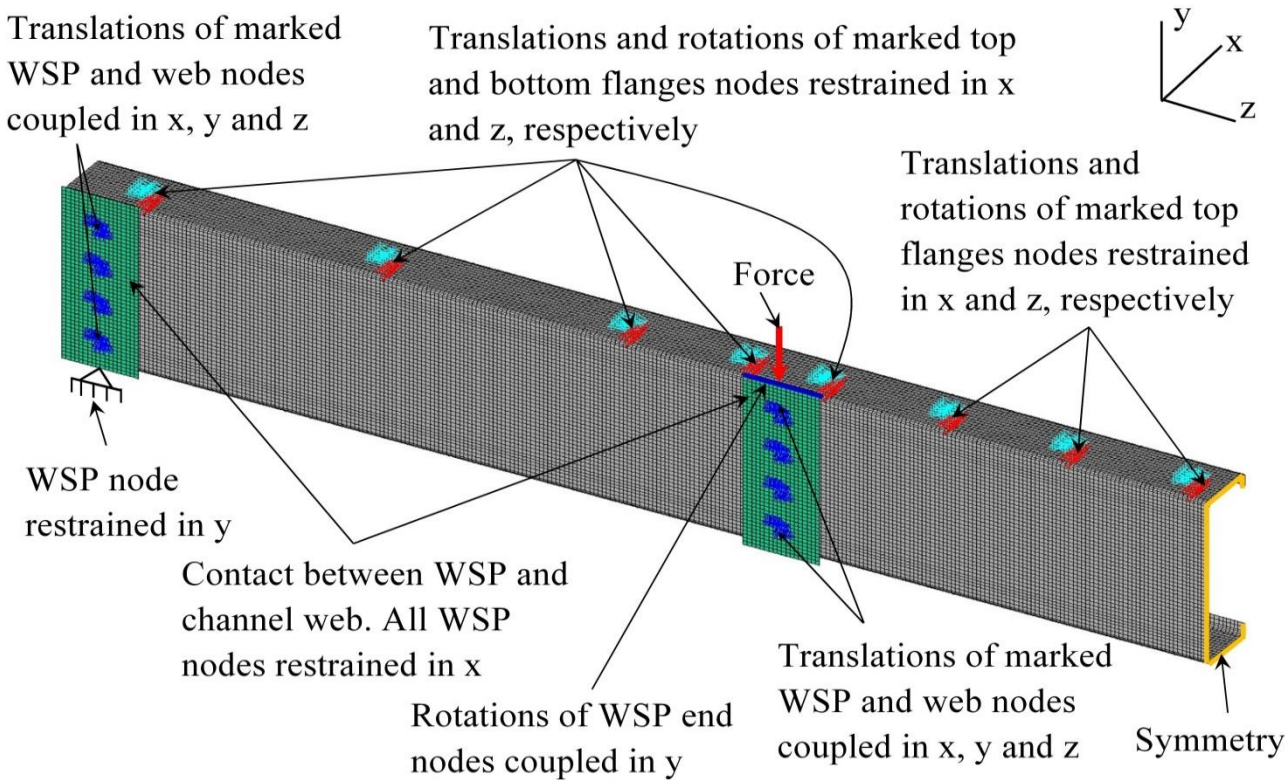

Fig. 4. Simulated boundary conditions in FE model to validate Pham and Hancock's [11] tests

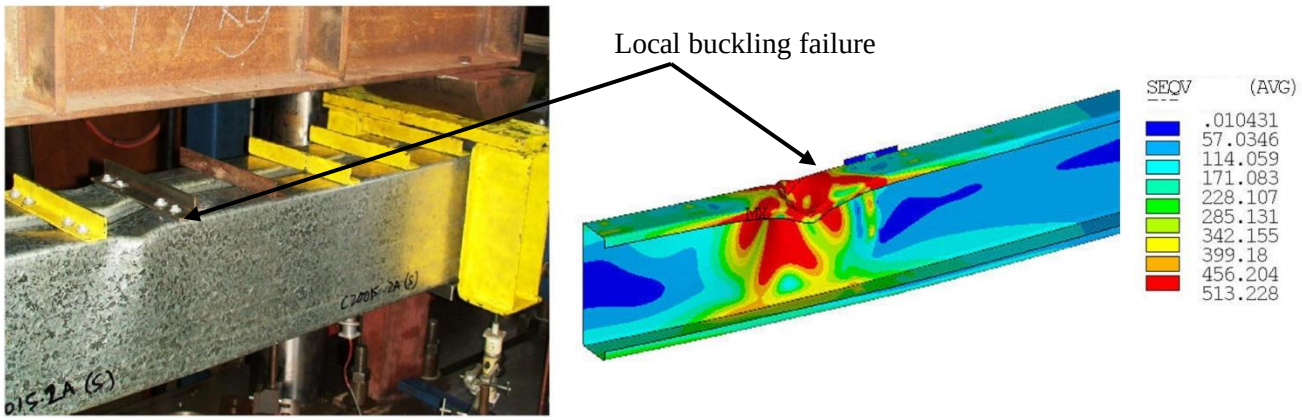

Fig. 5. Failure mode comparison between test [11] and FE model of the Specimen C20015-Ms

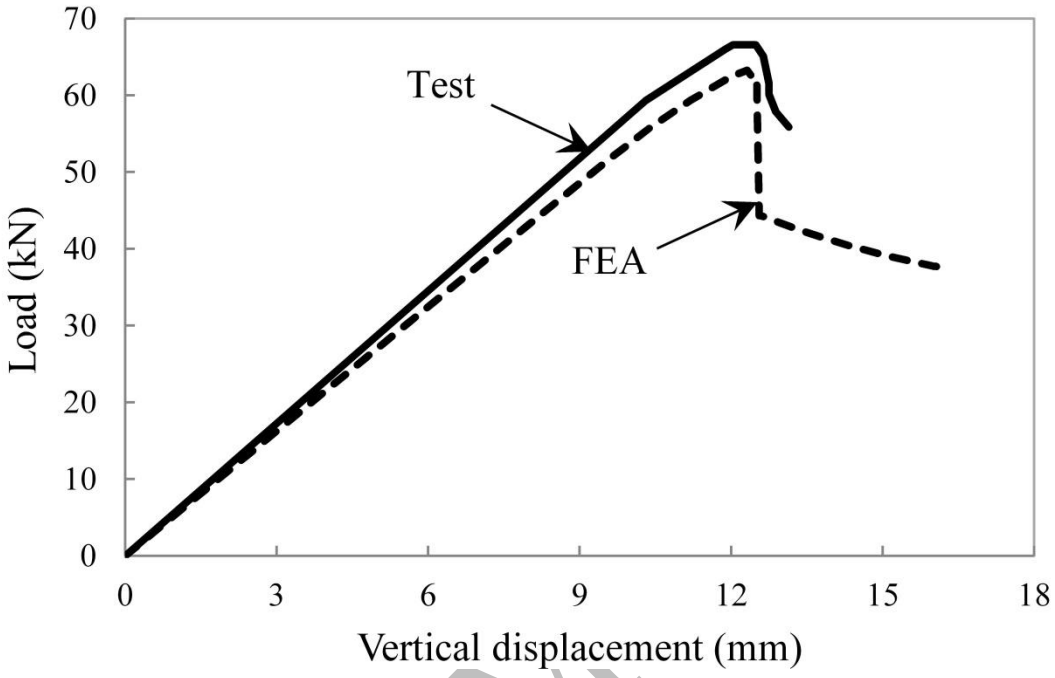

Fig. 6. Load-vertical displacement behaviour for the Specimen C20015-M from test [11] and FE analysis without initial geometric imperfection

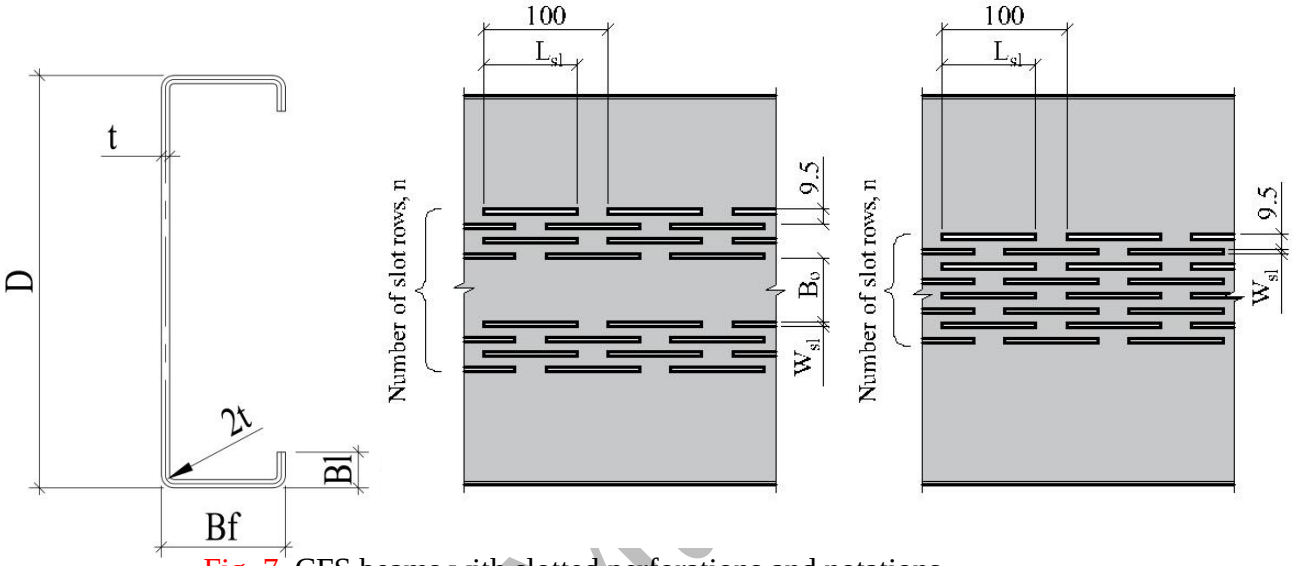

Fig. 7. CFS beams with slotted perforations and notations

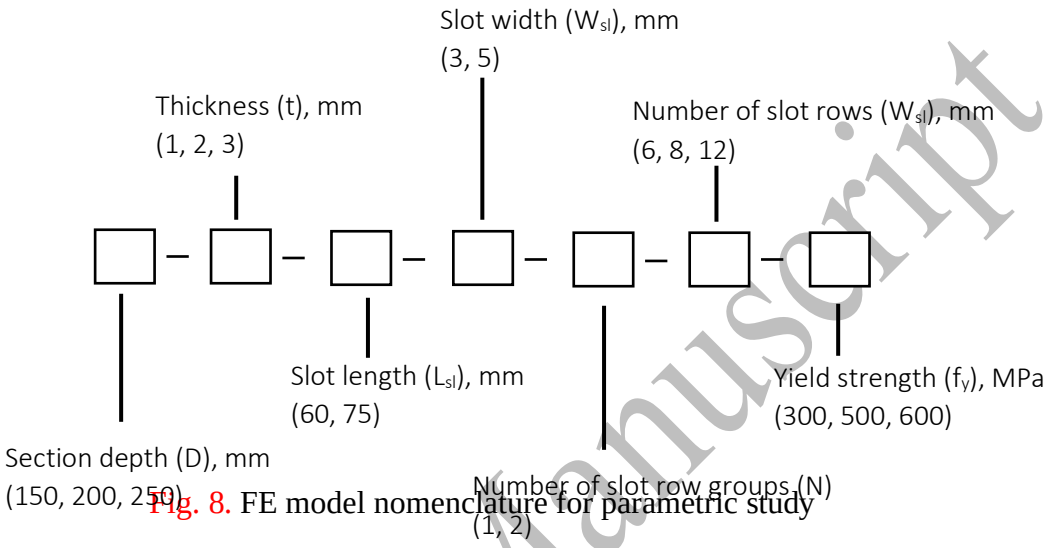

Fig. 8. FE model nomenclature for parametric study

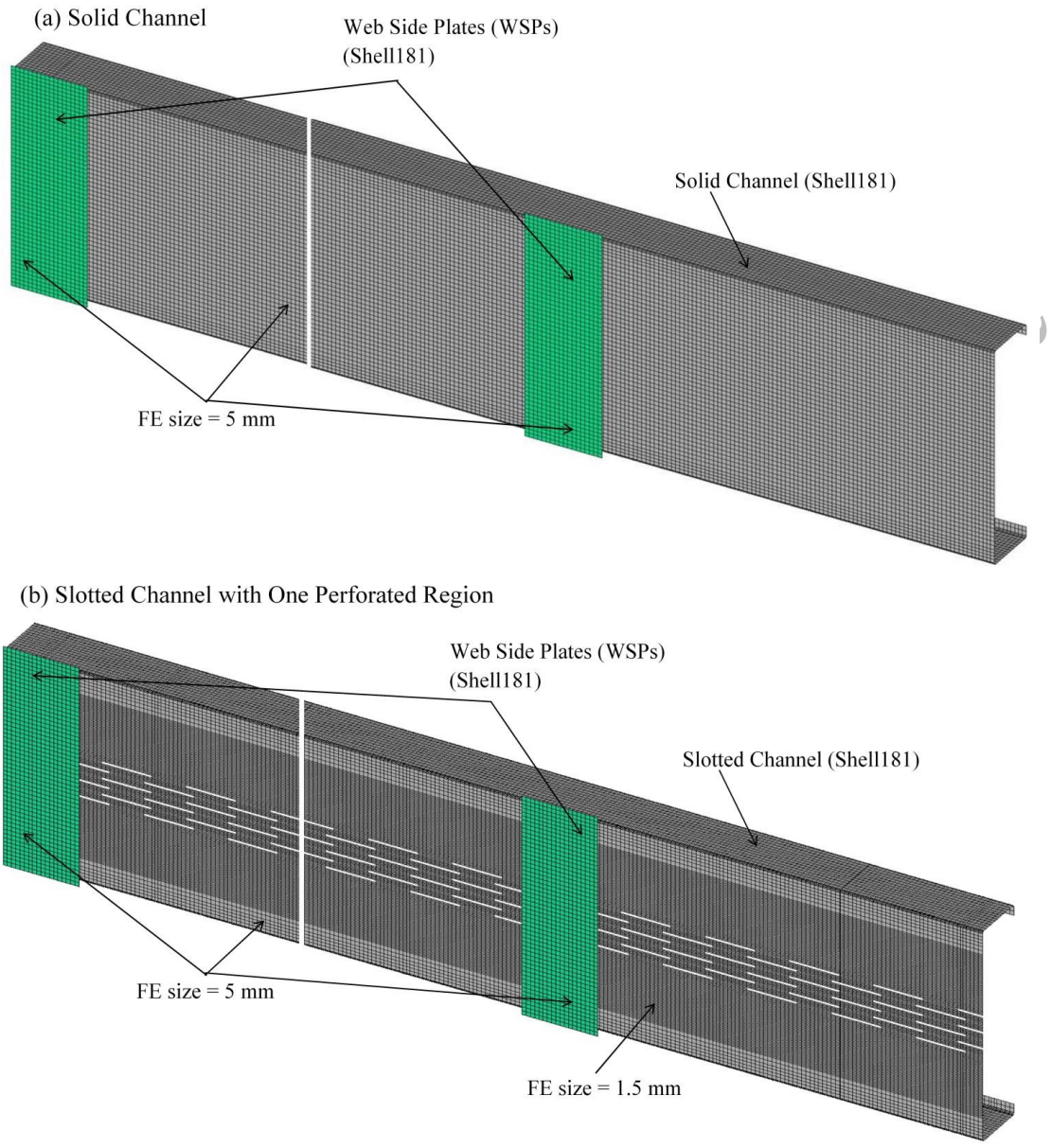

Fig. 9. FE models of 4800 mm long beam with staggered slotted perforations in the entire span

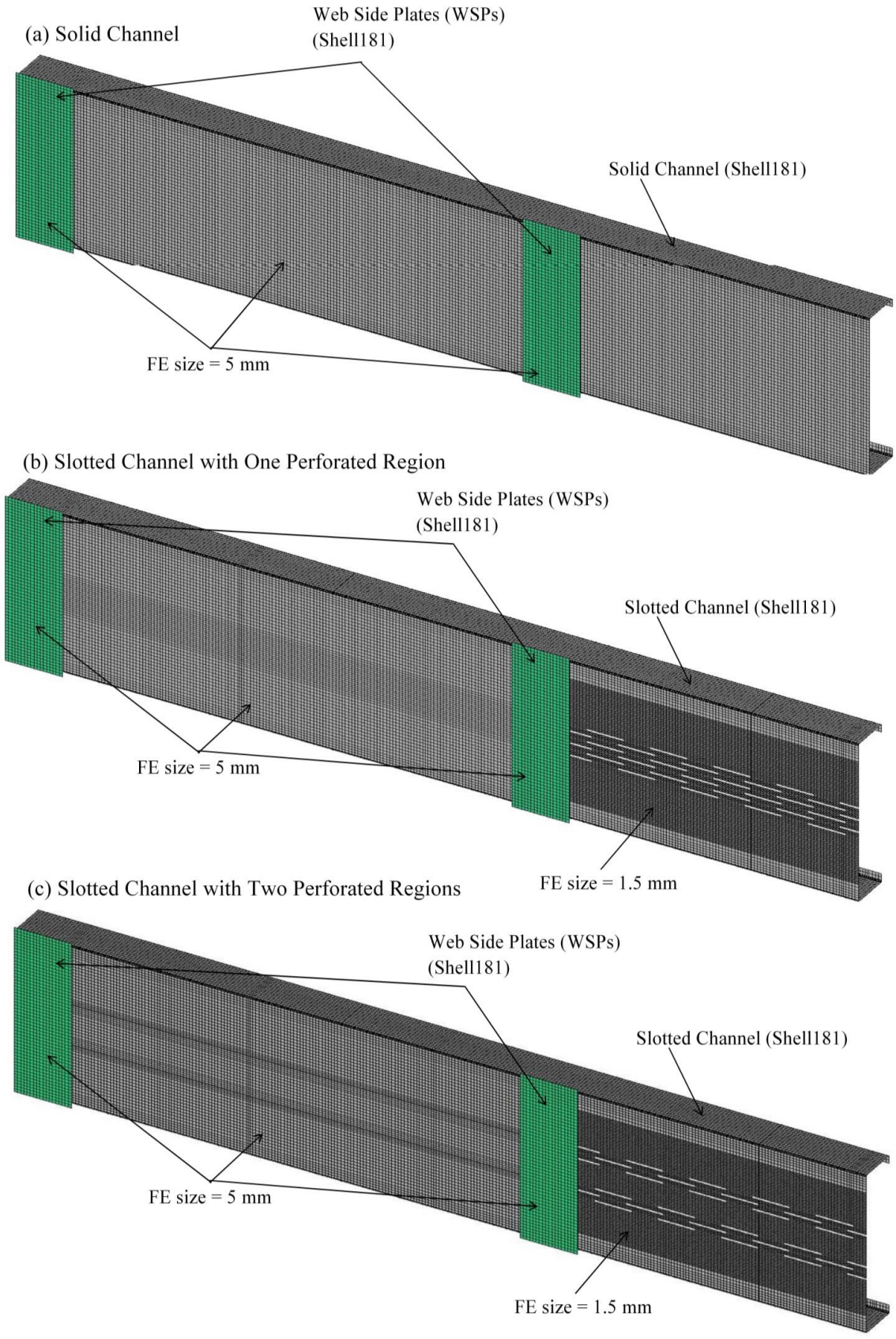

Fig. 10. FE models of 2600 mm long beam with staggered slotted perforations only in the mid-span (for parametric study)

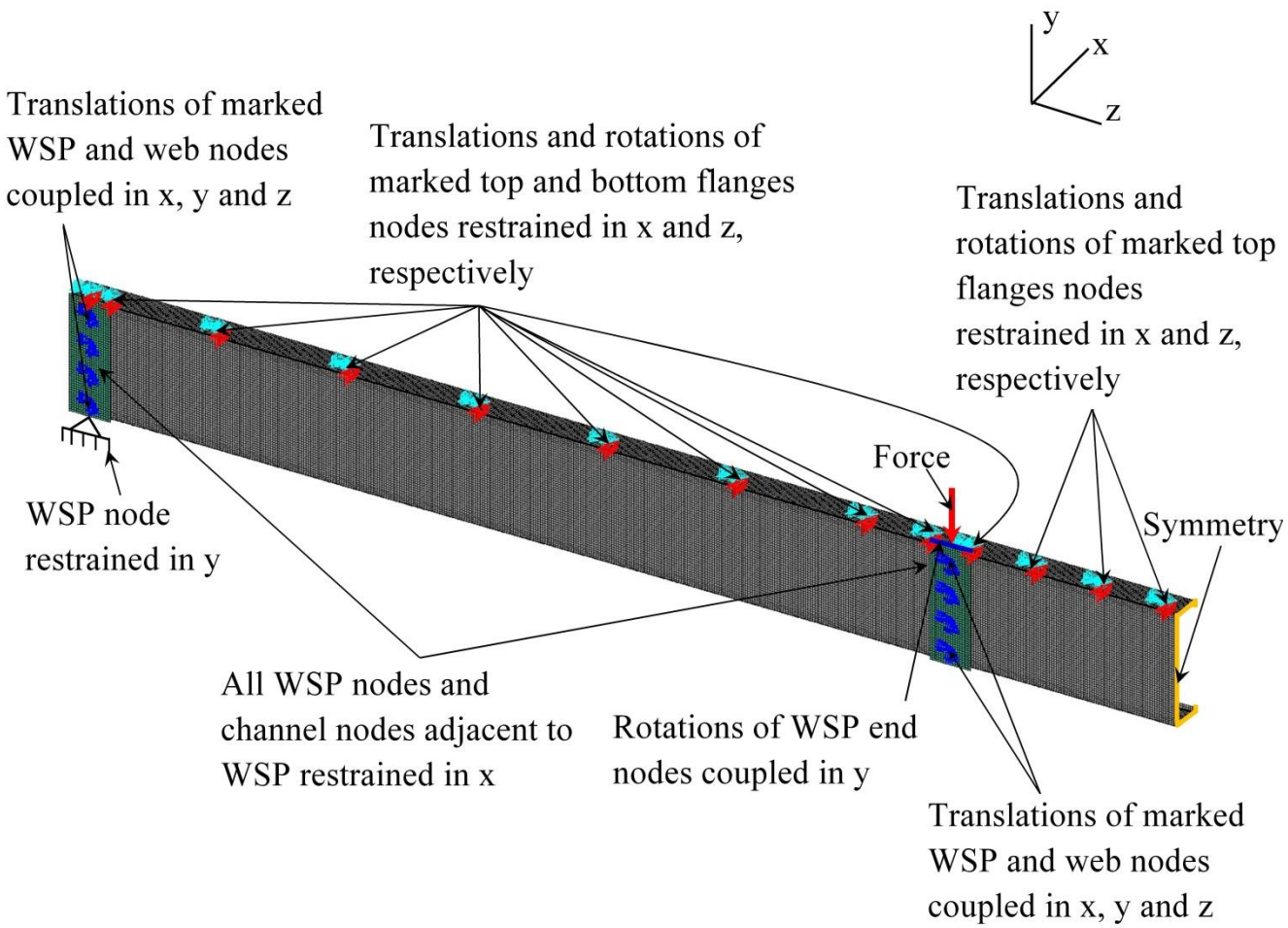

Fig. 11. Boundary conditions for FE models of 4800 mm long beams

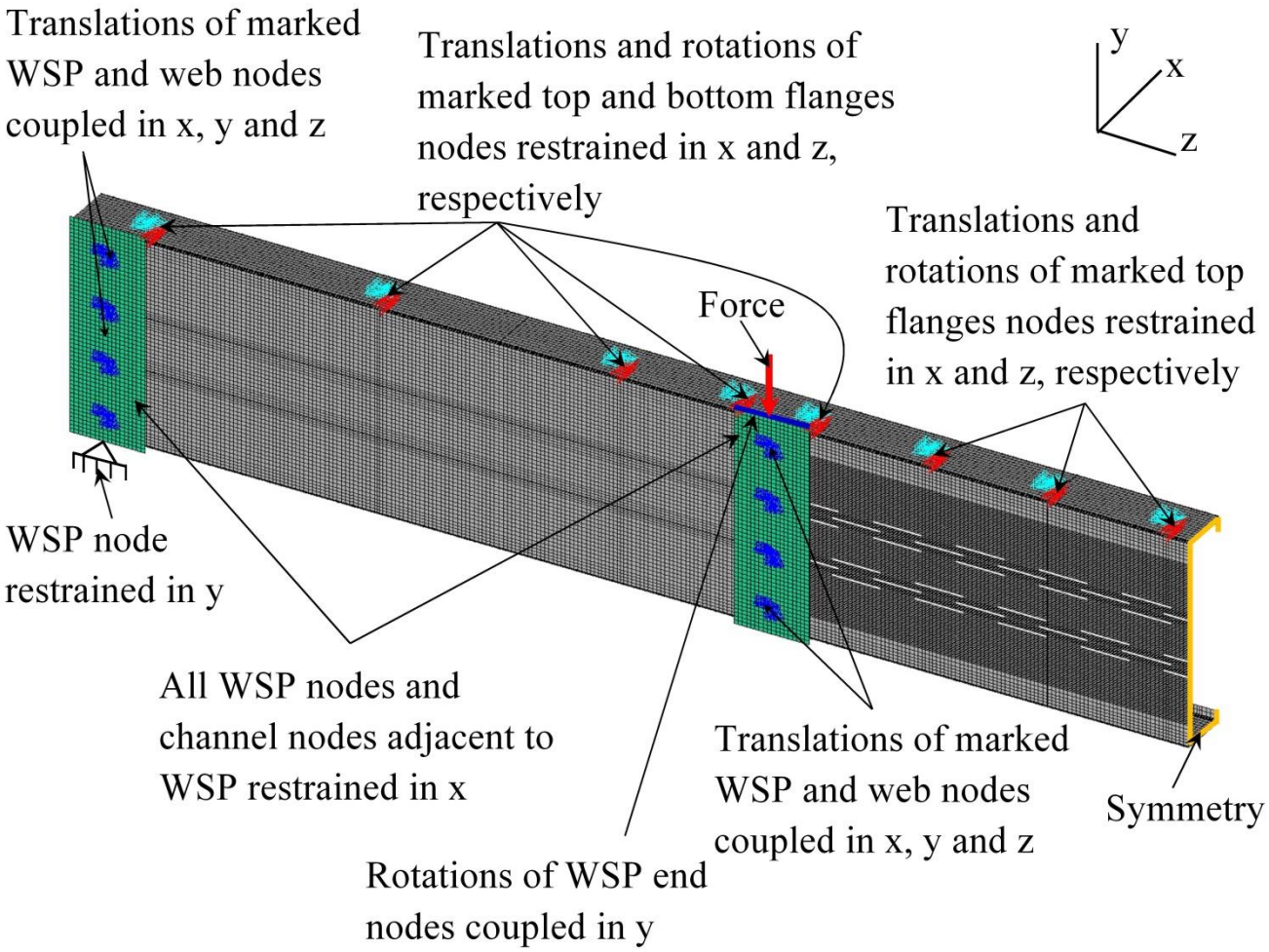

Fig. 12. Boundary conditions for FE models of 2600 mm long beams (for parametric study)

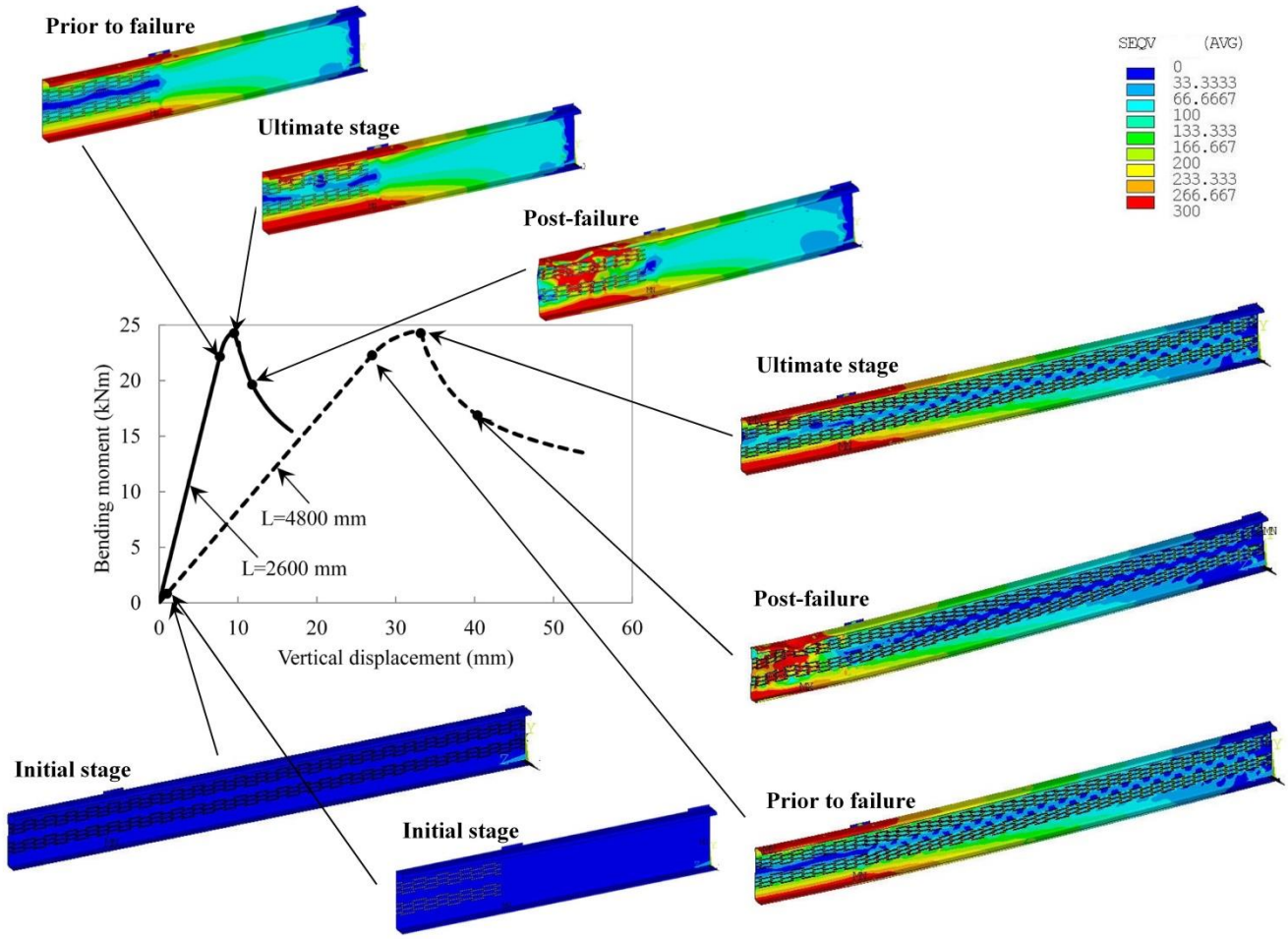

Fig. 13. Load-deflection plot of slotted channel 250-3-60-3-2-12-300 and its behavior at different stages.

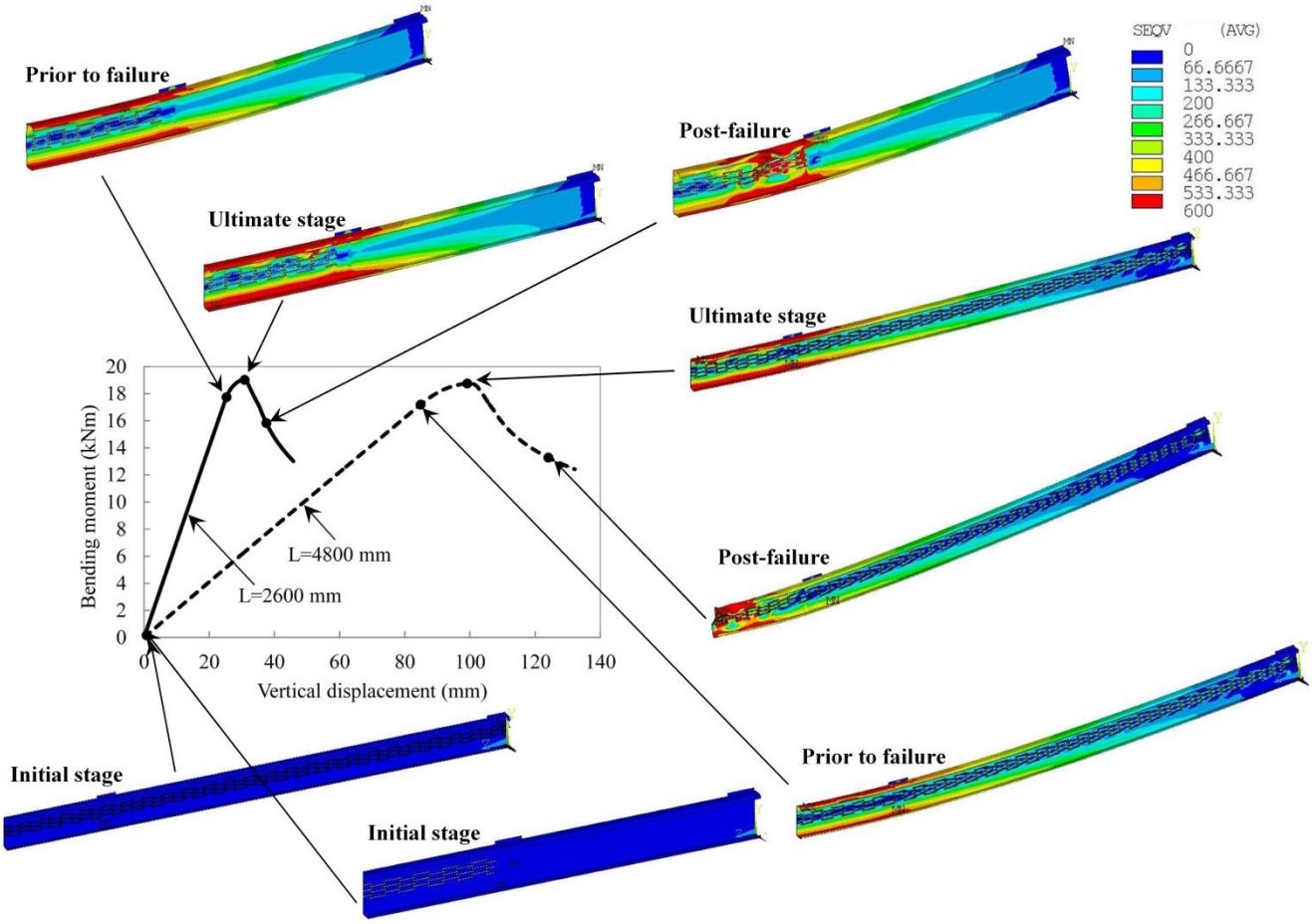

Fig. 14. Load-deflection plot of slotted channel 150-3-60-3-1-6-600 and its behavior at different stages.

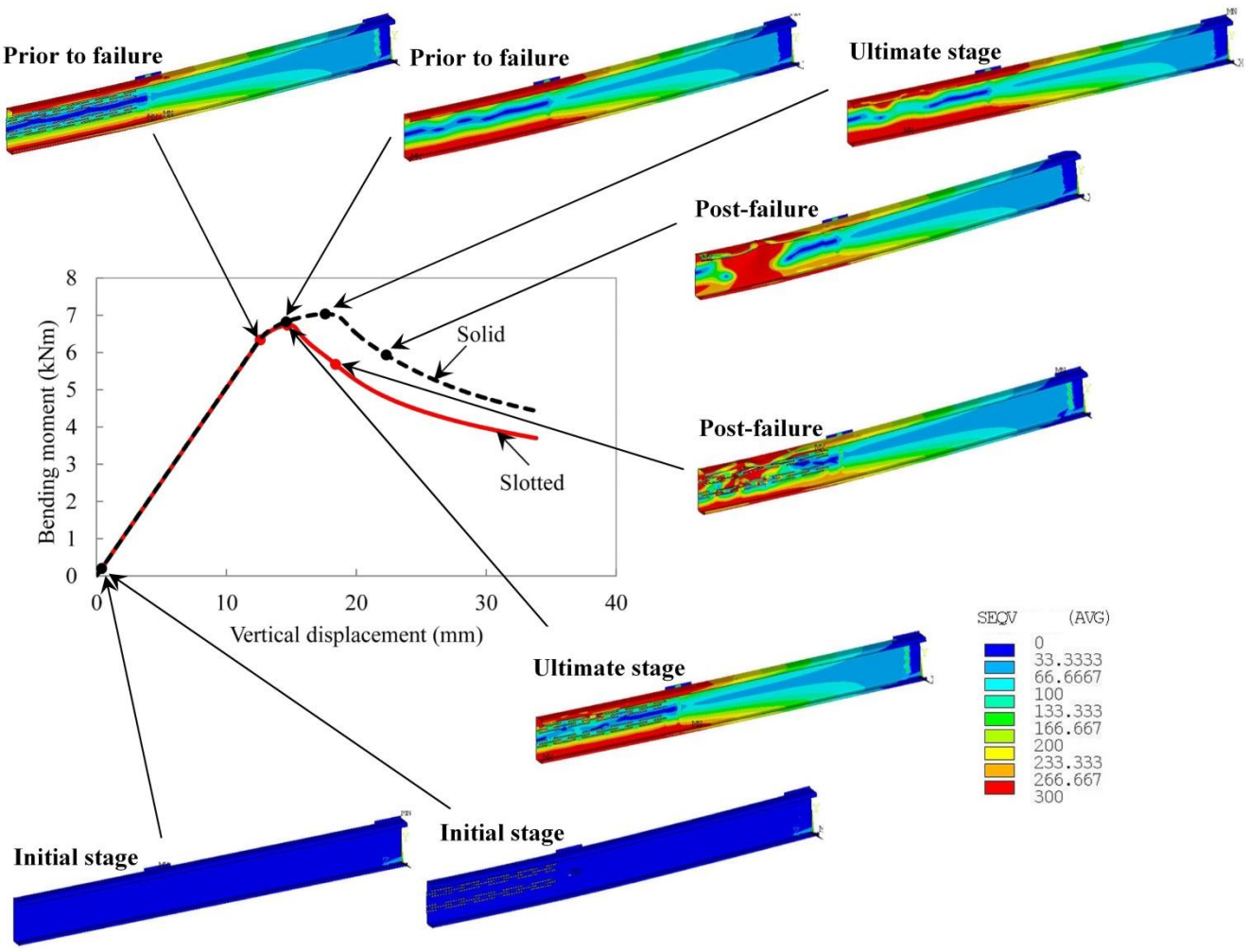

Fig. 15. Load-deflection plot of slotted channel 150-2-75-3-2-6-300 and solid channel 150-2-0-0-0-0-300 and their behavior at different stages.

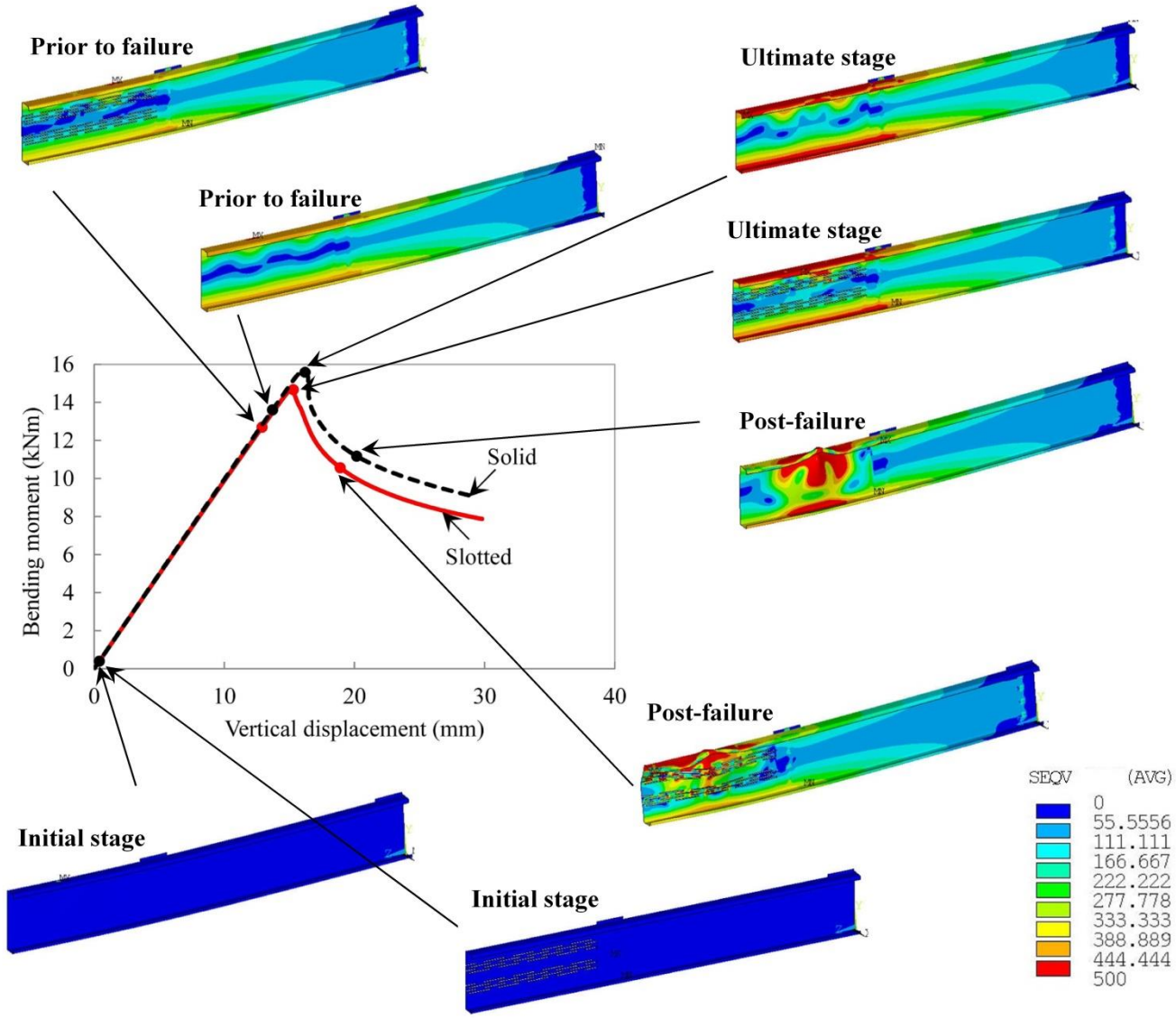

Fig. 16. Load-deflection plot of slotted channel 200-2-75-3-2-8-500 and solid channel 200-2-0-0-0-0-500 and their behavior at different stages.

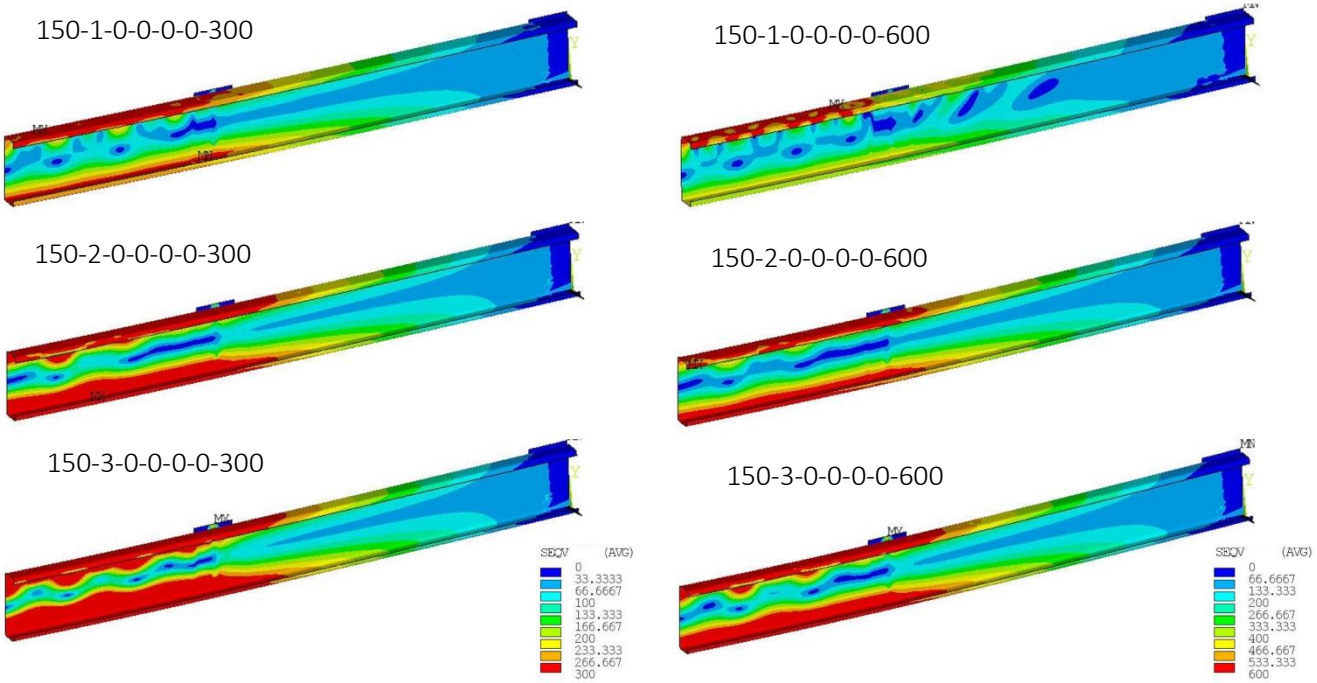

(a) Solid web CFS channels

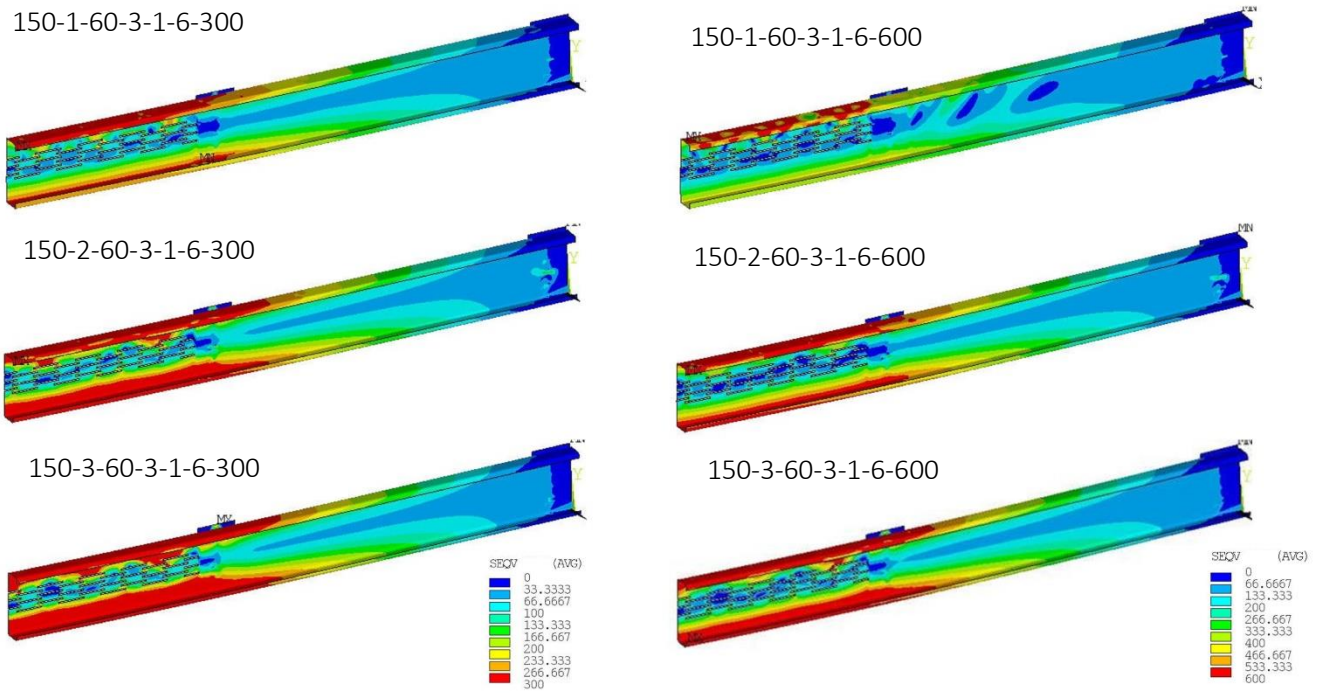

(b) Staggered slotted perforated channels

Fig. 17. Von misses stress failure pattern for 150 mm section depth solid and slotted perforated channels.

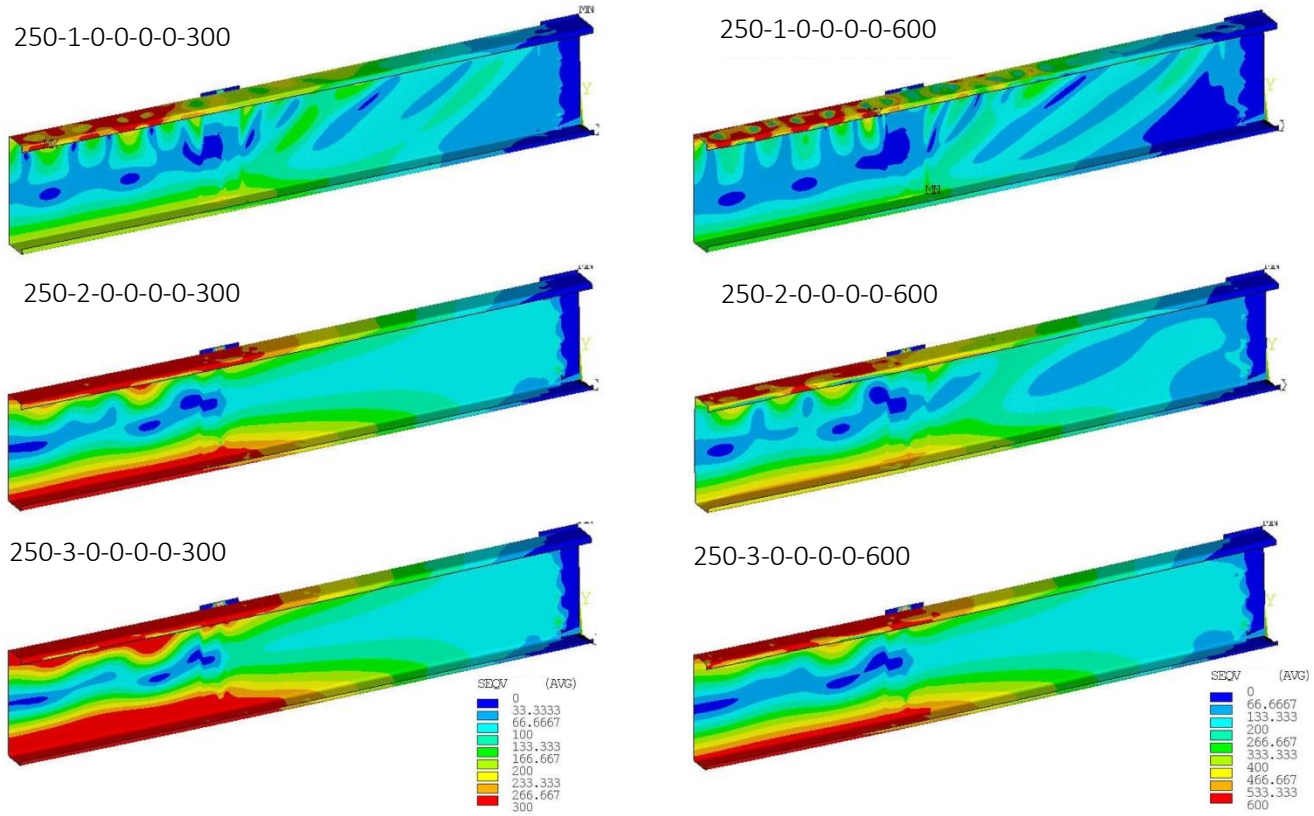

(a) Solid Channels

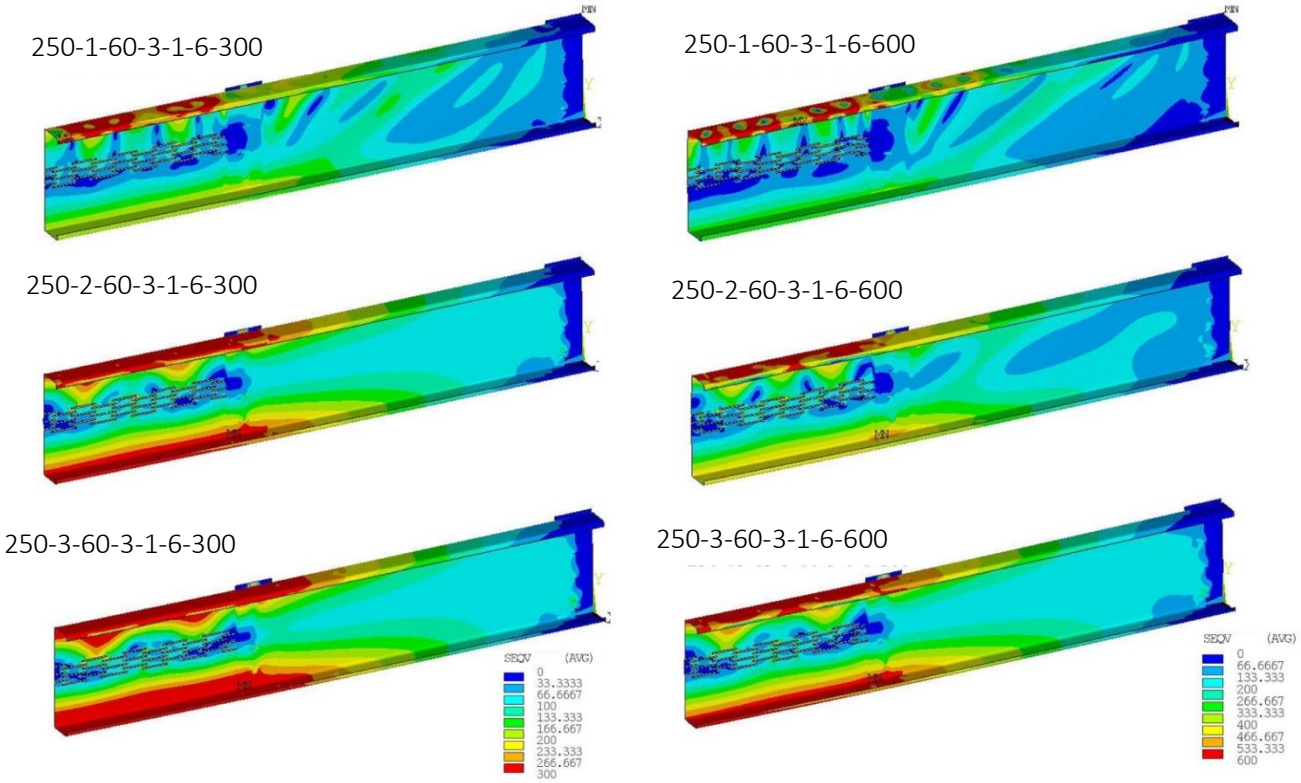

(b) Staggered slotted perforated channels

Fig. 18. Von misses stress failure pattern for 250 mm section depth solid and slotted perforated channels.

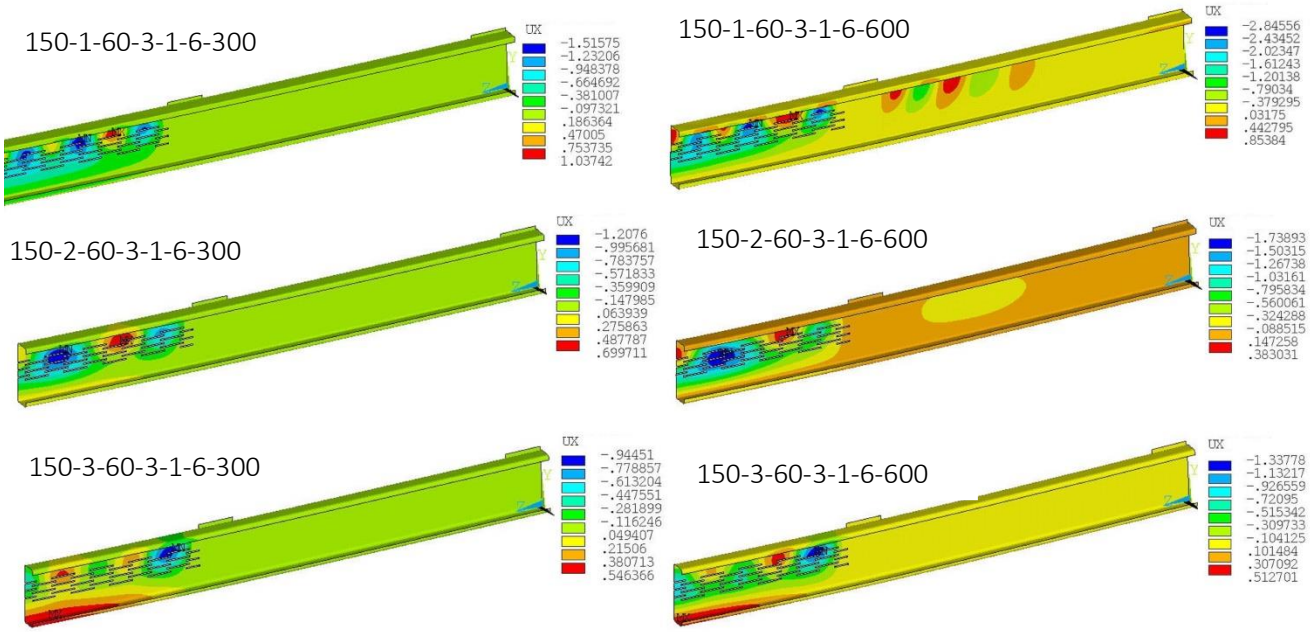

(a) 150 mm section depth CFS channels

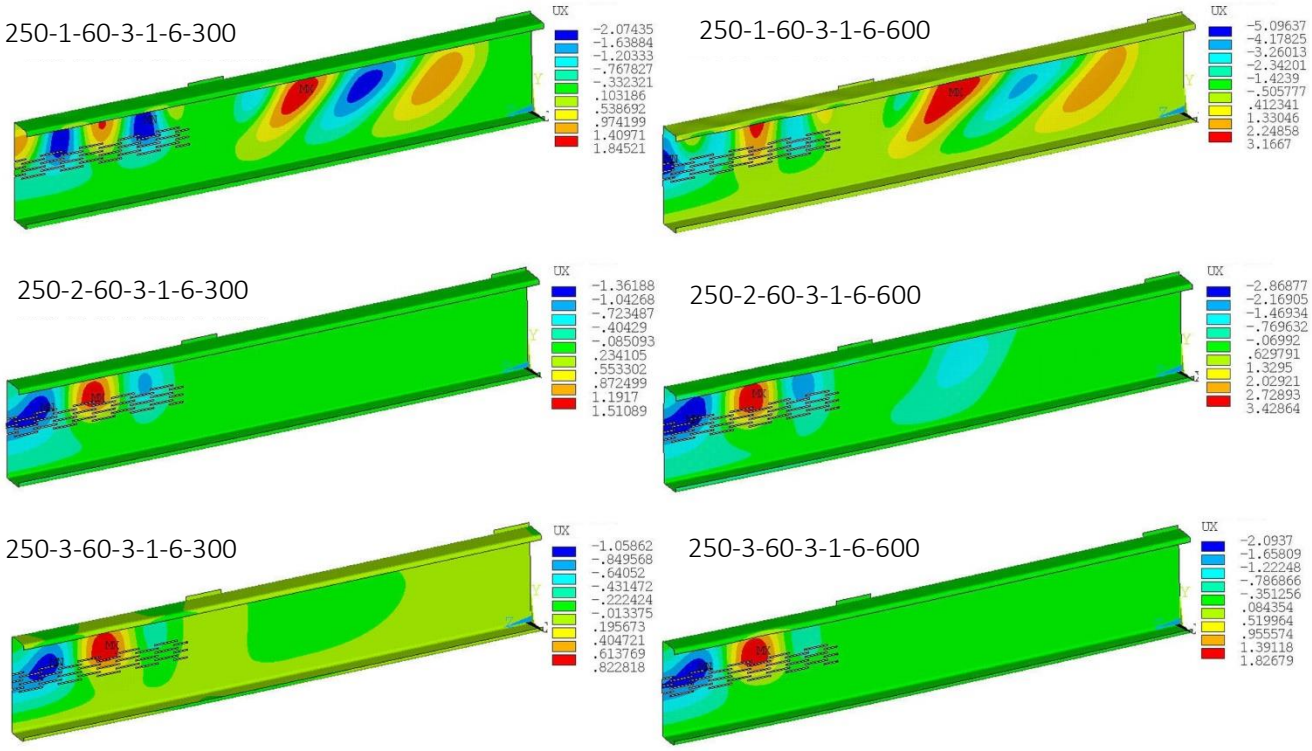

(b) 250 mm section depth CFS channels

Fig. 19. Deformation failure pattern of 150 and 250 mm section depth CFS channels with staggered slotted perforations

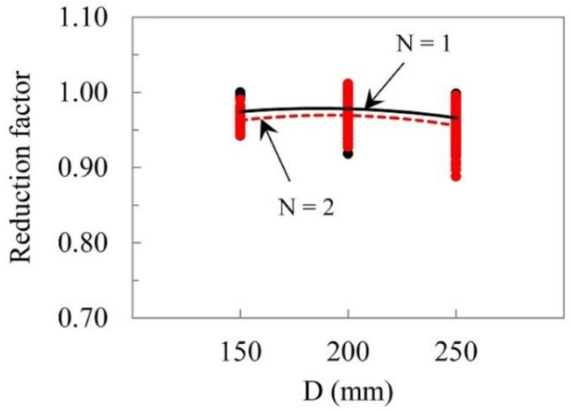

(a) Section depth

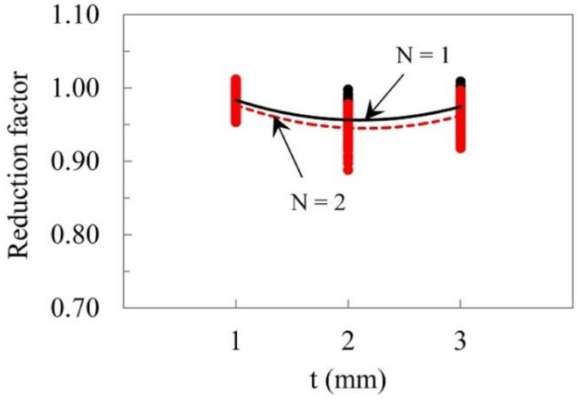

(b) Thickness

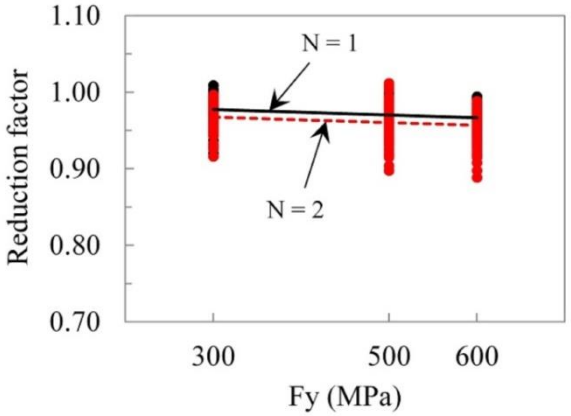

(c) Yield strength

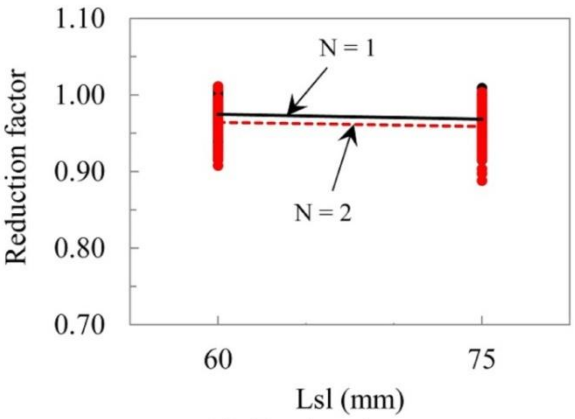

(d) Slot length

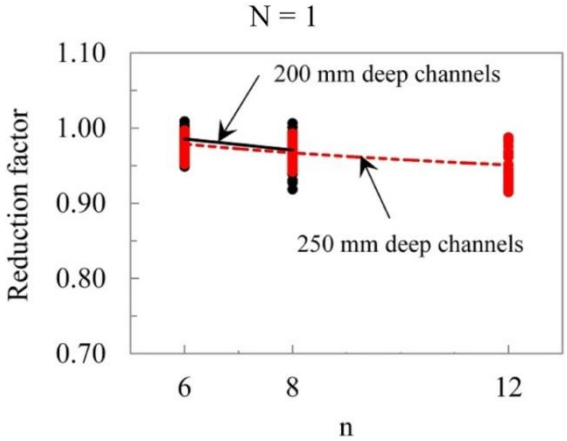

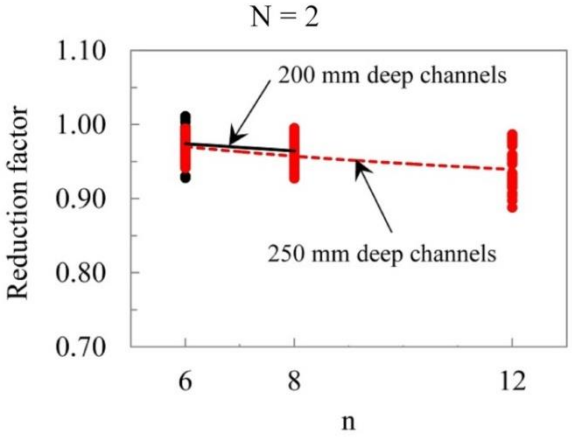

(e) Slot rows and slot row groups

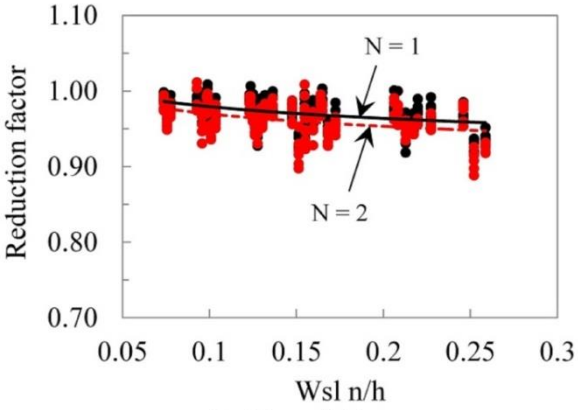

(f) Slot width

Fig. 20. Variation of reduction factor with varying parameters.

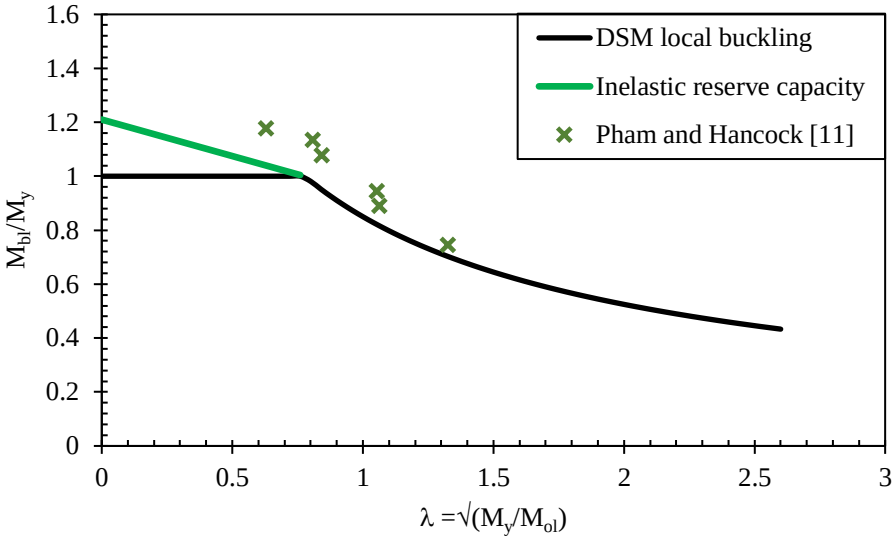

Fig. 21. DSM for solid CFS beams subject to local buckling and test results [11]

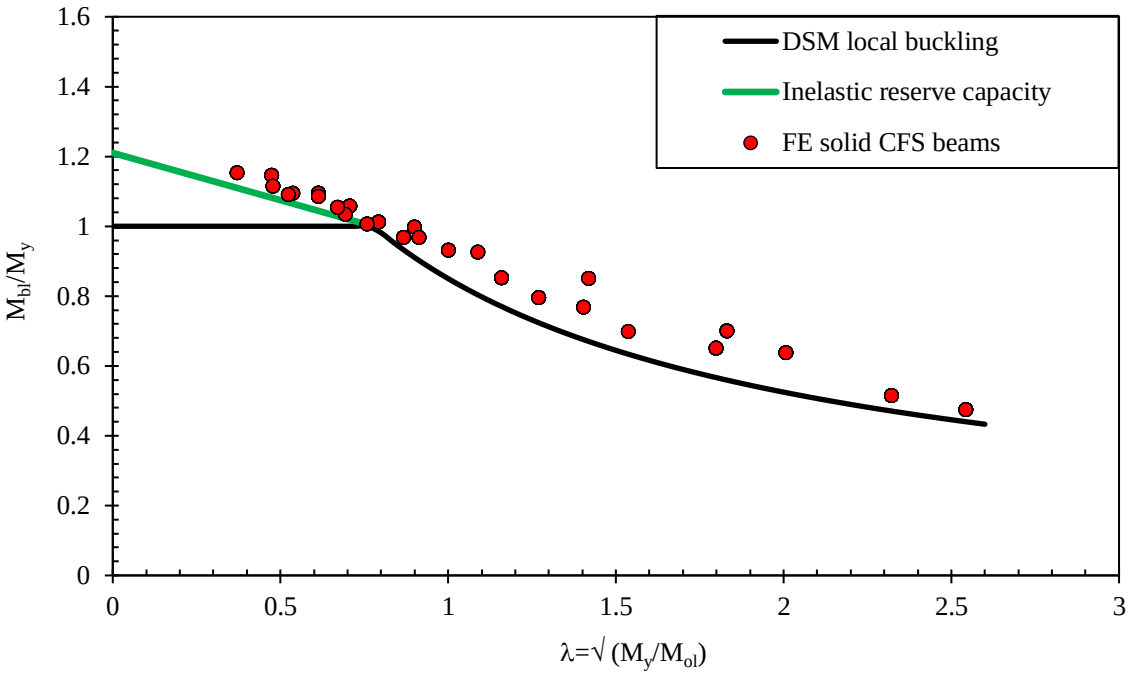

Fig. 22. FE capacity predictions for CFS solid web beams

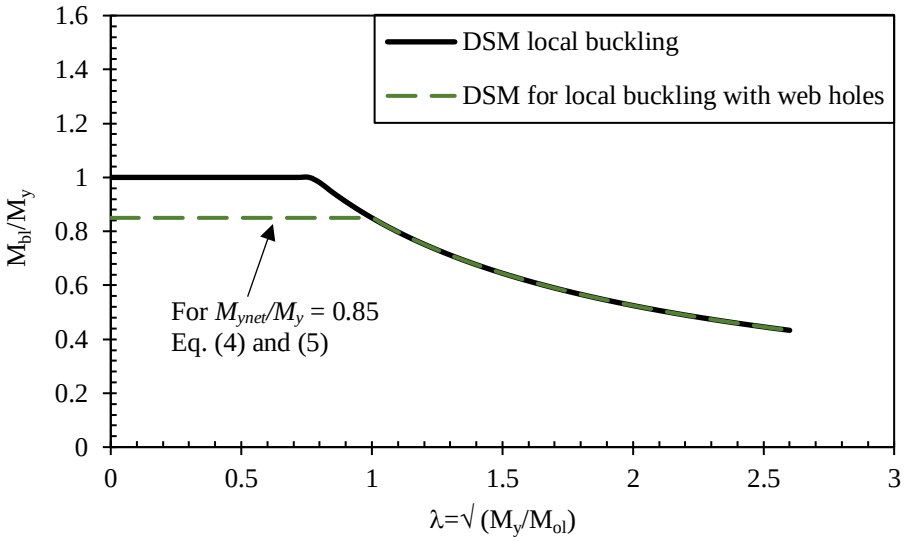

Fig. 23. DSM for CFS beams with web holes subject to local buckling

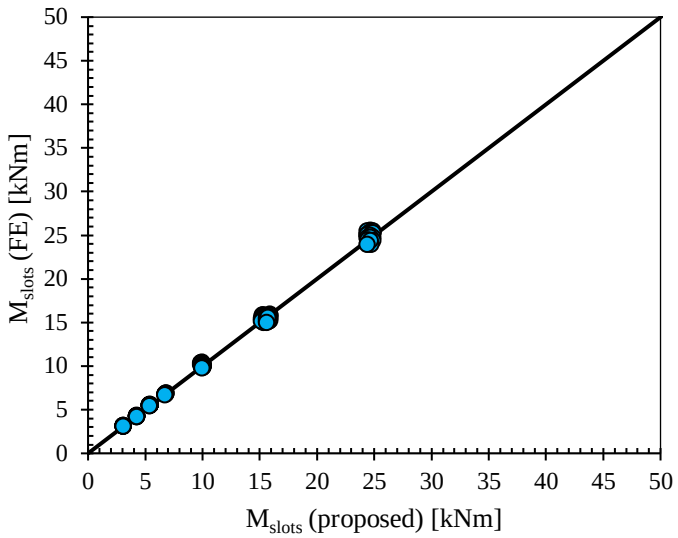

(a) f_y = 300 MPa

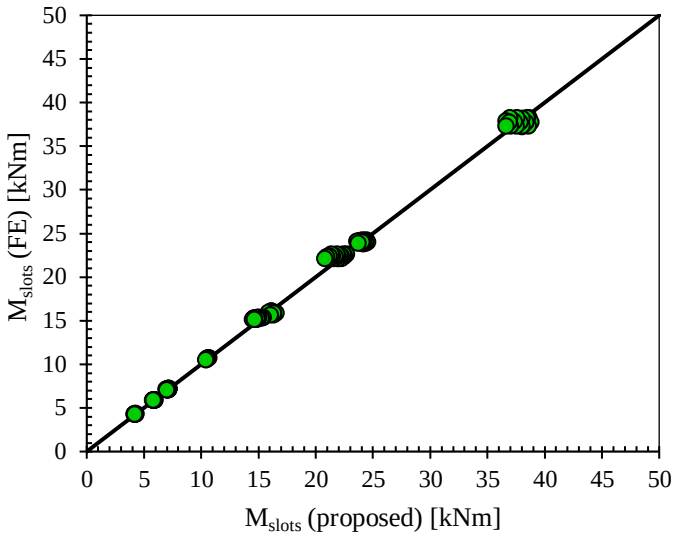

(b) f_y = 500 MPa

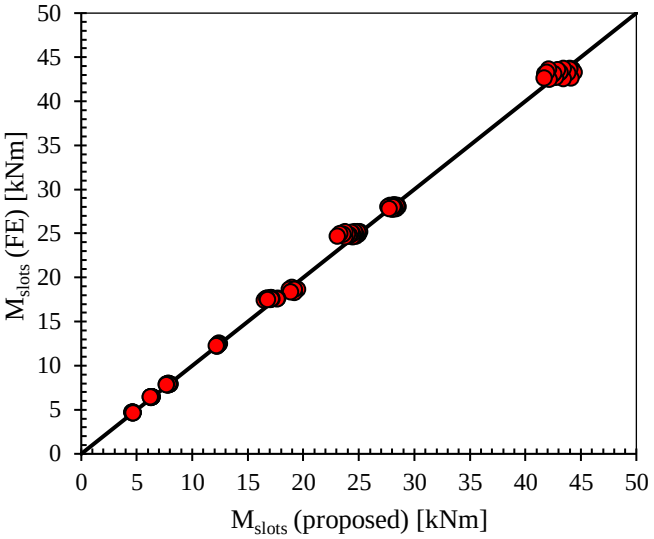

(c) f_y = 600 MPa

Fig. 24. Accuracy of the proposed reduction factor equation compare to the FE predictions

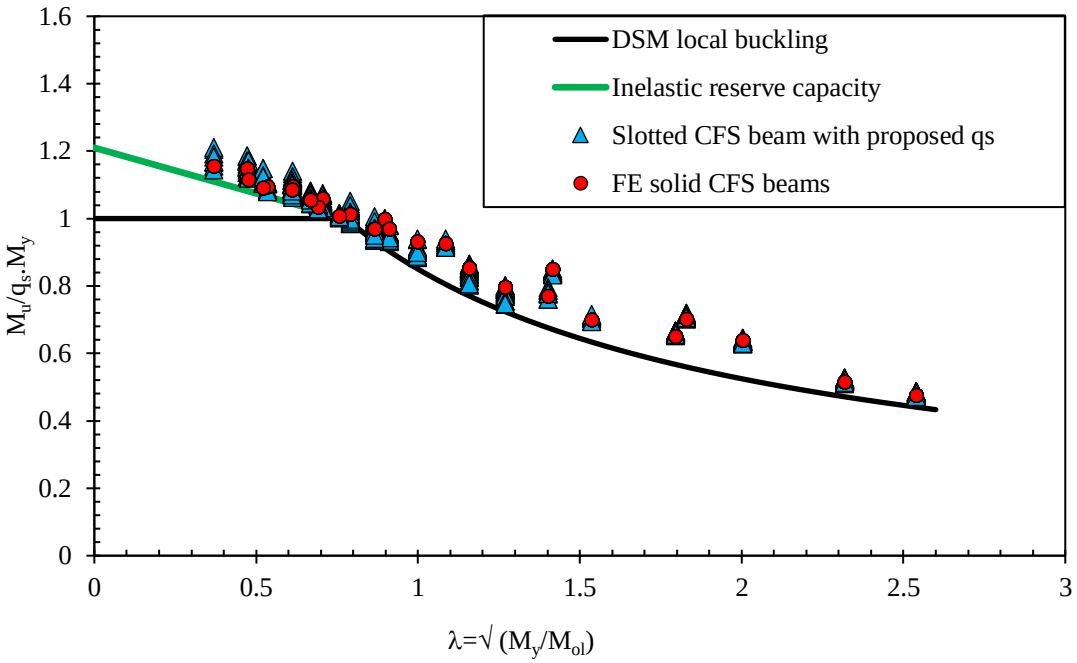

Fig. 25. Bending capacity predictions for slotted perforated beams with proposed q_s along with corresponding solid web beams